International Microbiology
https://doi.org/10.1007/s10123-026-00831-2

RESEARCH

Whole-genome analysis and enzymatic profiling of *Bacillus spizizenii* as a xylanase-producing source from Iran

Haniye Bigdeli[1] · Aboozar Soorni[1] · Mohammad Sedghi[2] · Rahim Mehrabi[1,5] · Maryam Fanaei[3] · Sadegh Zarei[4]

Received: 18 November 2025 / Revised: 9 April 2026 / Accepted: 17 April 2026

Abstract

Xylanases are crucial enzymes for the bioconversion of lignocellulosic biomass. Despite extensive studies on microbial xylanase producers, the identification of new indigenous strains with enhanced enzyme activity remains a significant challenge. While there is some existing research on the isolation of xylanase-producing bacteria from Iran, our study specifically aimed to comprehensively isolate and characterize novel xylanase-producing bacterial strains from a diverse range of samples collected across the region. A total of 26 samples were collected from various regions of Iran. From these, 18 distinct bacterial isolates were obtained based on colony morphology. Among these, 13 isolates showed clear zones of xylan hydrolysis in the qualitative screening, indicating xylanase activity. Among these isolates S3 and S4 exhibited superior enzyme production. Strain S3 showed the highest activity of 11.56 U/mL at pH 9 and 40 °C, while S4 achieved 9.35 U/mL at pH 9 and 50 °C. Notably, S3 maintained significant activity across a broad pH range (pH 4–9), highlighting its adaptability. Molecular and phylogenetic analyses revealed these isolates to be previously uncharacterized, xylanase-producing variants of *Bacillus spizizenii* originating from Iran. Whole-genome sequencing of S3 revealed unique xylanase genes from the GH11 and GH43 families. Molecular docking indicated favorable substrate-binding affinities with the *xynA1* (GH11) gene showing the strongest interaction with xylan (-9.4 kcal/mol), supported by kinetic parametersThese findings present new *B. spizizenii* strains as promising candidates for industrial applications, particularly where broad pH adaptability is required, and provide a genetic foundation for future enzyme engineering.

Keywords Xylanase · *B. spizizenii* · PH adaptability · GH11 and GH43 families · Docking

Introduction

Xylanases are essential enzymes that catalyze the hydrolysis of xylan, a major hemicellulose component found in plant cell walls, breaking it down into smaller oligosaccharides and xylose. Xylan is one of the most abundant biopolymers on Earth, second only to cellulose, and is composed of xylose, arabinose, mannose, and galactose, depending on the source (Ebringerová and Heinze 2000). Xylanases are classified as endo-1,4-β-xylanases (EC 3.2.1.8), which mainly belong to the glycoside hydrolase families GH10 and GH11, based on their catalytic mechanism and sequence homology (Collins et al. 2005; Pollet et al. 2010; Paës et al. 2012; Lombard et al. 2014). GH10 xylanases exhibit a (β/α)8-barrel fold in their catalytic domain and possess broad substrate specificity, making them efficient in hydrolyzing both linear substrates and substituted forms of xylan. These enzymes are capable of cleaving glycosidic bonds via a double-displacement mechanism, producing

✉ Aboozar Soorni
soorni@iut.ac.ir

[1] Department of Biotechnology, College of Agriculture, Isfahan University of Technology, Isfahan, Iran

[2] Department of Animal Sciences, College of Agriculture, Isfahan University of Technology, Isfahan 84156-83111, Iran

[3] Department of Food Science and Technology, College of Agriculture, Isfahan University of Technology, Isfahan 84156-83111, Iran

[4] Present address: Department of Plant Protection, College of Agriculture, Isfahan University of Technology, Isfahan 84156-83111, Iran

[5] Keygene N.V, Wageningen 6700 AE, The Netherlands

Published online: 24 April 2026

shorter xylooligosaccharides (XOS) and D-xylose as products (Lo Leggio et al. 1997; Pollet et al. 2010; Hori et al. 2013; Lombard et al. 2014; Lin et al. 2018; Rahmani et al. 2019). In contrast, GH11 xylanases are highly specialized β−1,4 endoxylanases with narrow substrate specificity, targeting the internal β−1,4 glycosidic bonds in xylan. GH11 enzymes can be categorized as acidic or basic xylanases based on their pH optima and the nature of residues adjacent to their acid/base catalysts (Pollet et al. 2010; Paës et al. 2012; Moreira and Filho 2016; Yagi et al. 2019). Meanwhile, GH43 xylanases predominantly function as exo-β-xylosidases, breaking down xylan and xylooligosaccharides from their non-reducing ends. (Mai et al. 2000; Morana et al. 2007; Morais et al. 2021; Pereira de Almeida et al. 2022; Saleh et al. 2022).

Xylanases are used in food processing, animal feed, and biofuel production for their ability to improve bakery texture, aid juice clarification, and enhance pulp bleaching efficiency (Beg et al. 2001; Bhardwaj et al. 2019). However, their effectiveness is limited by sensitivity to pH and temperature, with optimal activity typically between pH 5.0 to 9.0 and temperatures of 50 °C to 80 °C (Walia et al. 2013; Robledo et al. 2016). Microbial sources, especially *Bacillus* species and filamentous fungi like *Aspergillus* and *Trichoderma*, provide diverse xylanases. Fungal xylanases are preferred in acidic food conditions, while bacterial xylanases are better for high-temperature applications (Thomas et al. 2017; Dodda et al. 2021; Pasalari and Homaei 2022; Gavande et al. 2024). For example, fungal xylanases are often favored in the food industry for their efficiency in acidic conditions, whereas bacterial xylanases are more suited for high-temperature applications such as bioethanol production (Hung et al. 2011; Yang and Han 2018). To further harness the potential of xylanases, researchers can explore various environments to isolate novel bacterial and fungal strains with desirable enzymatic characteristics tailored to specific applications. Alternatively, engineering microbial strains to enhance xylanase properties such as stability, activity range, or substrate specificity presents a complementary approach. While strain isolation offers a faster and more cost-effective solution, genetic engineering provides long-term possibilities for overcoming the limitations of natural enzymes.

The identification of microbial strains capable of producing extracellular xylanase has advanced significantly in recent years. For instance, soil samples collected from the Rajshahi University campus yielded a strain identified as *Bacillus cereus* through *16 S* rRNA gene sequencing, demonstrating substantial extracellular xylanase activity and underscoring the potential of soil-derived microbes in enzyme production (Roy and Habib 1970). Similarly, isolation efforts from a salt farm environment revealed a *Bacillus pumilus* strain capable of producing alkaline xylanase, showcasing the versatility of xylanase-producing bacteria in adapting to and thriving within diverse environmental conditions (Menon et al. 2010). The discovery of thermoalkalophilic strains has advanced xylanase research. *Bacillus arseniciselenatis* DSM 15,340 produced efficient xylanase during solid-state fermentation with wheat bran, showing optimal activity at 50 °C and pH 8, underscoring the importance of tailored fermentation conditions (Kamble and Jadhav 2012). Exploration of the Western Ghats region in Kerala uncovered *Bacillus amyloliquefaciens* XR44A, a microorganism with both cellulolytic and xylanolytic capabilities. This strain produced endo-1,4-β-xylanase with notable stability and enzymatic activity, highlighting the value of diverse ecosystems in uncovering strains with industrially relevant enzyme profiles (Amore et al. 2015). Recent investigations into black soil microbiota identified *B. subtilis* SSMK413 as a robust co-producer of cellulase and xylanase (Shah et al. 2025), and the human gut microbiome has been tapped for a cold-active xylanase from *Paenibacillus* sp. XP01 (Gao et al. 2025). Concurrently, significant efforts are focused on engineering xylanases for enhanced properties; for instance, the thermostability of GH11 xylanases from *Streptomyces lomondensis* and *Alteromonas macleodii* has been successfully improved through terminal sequence substitution and modular mosaic assembly, respectively (Deng et al. 2025; Wang et al. 2025). Thermophilic microorganisms have been particularly impactful in enzyme research. *Clostridium thermocellum* was shown to produce a heat-resistant endoxylanase, *Xyn141E*, belonging to the GH141 family. This enzyme demonstrated exceptional thermal stability and enzymatic activity under a range of pH and temperature conditions, making it highly suitable for high-temperature industrial applications (Heinze et al. 2017).

Given the various factors that influence xylanase activity, it remains vital to discover new microbial strains capable of producing high levels of stable enzyme for specific industrial applications. Despite extensive studies on *Bacillus*-derived xylanases, reports on indigenous Iranian strains remain limited, particularly those combining comprehensive enzymatic characterization with genome-scale and structural analyses. Most previous studies have focused either on isolation and basic enzymatic screening or on genetic characterization without functional validation. Furthermore, xylanases with broad pH adaptability, a highly desirable trait for diverse industrial applications, are rarely reported from Iranian

microbial resources. This study addresses this gap by isolating and characterizing novel xylanase-producing bacteria from diverse environmental and industrial samples across Iran, including soils, organic fertilizers, food sources, and effluents. The isolated strains were screened qualitatively and quantitatively. The most potent producers underwent enzyme purification, stability assessments under varying pH and temperature conditions, and morphological and molecular characterization. Furthermore, whole-genome sequencing and in silico analyses, including molecular docking, were employed to identify and characterize the key xylanase genes, exploring their physicochemical properties, structural features, and catalytic potential.

Materials and methods

Sampling and isolation of xylanase-producing strains

To identify high-potential xylanase-producing strains, screening experiments were conducted on microbial strains purified from twenty-six samples collected from various regions of Iran. These regions and sample types were selected based on previous research and their potential for harboring xylanase-producing microorganisms (Singh et al. 2010; Nkohla et al. 2017; Kumar et al. 2018; Shanthi and Roymon 2018). The samples were collected in sterile tubes and transported to the laboratory under 4 °C condition for further analysis (Shanthi and Roymon 2018). To isolate xylanase-producing microbial strains, one gram of each sample was suspended with saline solution (0.9% NaCl) and then was serially diluted up to 10^{-5} in distilled water and thoroughly mixed using a vortex (Sapkota et al. 2020). A 100 µL aliquot of each dilution was spread onto Luria Broth (LB)-agar plates, which were incubated at 37 °C for 24 h. The isolated bacterial strains were subsequently cultured on a selective medium containing beechwood xylan (Sigma Aldrich, CAS: 9014-63−5) (5 g peptone, 20 g agar, 5 g NaCl, 0.5 g $MgSO_4$, 0.15 g $CaCl_2$, 10 g xylan, and 500 mL sterile distilled water (SDW) with pH 7 and then incubated at 30 °C for 48 h (Pasalari and Homaei 2022). Following incubation, the plates were stained with 5 mL of Gram's iodine solution (2.0 g KI and 1.0 g iodine dissolved in 300 mL SDW) for 5 min to visualize clear zones, indicating xylan degradation (Kasana et al. 2008). Xylanase activity in the qualitative assay was assessed by calculating the potency index (PI)(Luong et al. 2023).

Enzyme activity assay

Bacterial strains exhibiting the largest clear zones in the initial screening were selected for secondary screening and subsequent xylanase activity assays. The selected strains were cultured in LB broth and incubated at 37 °C with continuous shaking at 150 rpm for 24, 48, and 72 h. Following incubation, the cultures were centrifuged at 12,000 × g for 20 min at 4 °C to separate the cells from the supernatant. The supernatant was collected and used as the crude enzyme extract for further analysis. Xylanase activity (expressed in units per milliliter, U/mL) was quantified using the dinitrosalicylic acid (DNS) method, which measures the release of reducing sugars from xylan hydrolysis (Chen et al. 2016). For the assay, 500 µL of the crude enzyme solution was mixed with 1 mL of 0.5% (w/v) xylan substrate prepared in 50 mM sodium phosphate buffer (pH 6.0). The reaction mixture was incubated at 50 °C for 10 min, after which the reaction was terminated by adding 3 mL of DNS reagent. The mixture was then boiled at 100 °C for 5 min to develop the colorimetric reaction and subsequently cooled to room temperature. The absorbance of the resulting solution was measured at 540 nm using a spectrophotometer (Pasalari and Homaei 2022). A standard curve was generated using known concentrations of xylose (0.1–1.0 mg/mL) to correlate absorbance values with the amount of reducing sugars released. One unit of xylanase activity (U/mL) was defined as the amount of enzyme required to liberate 1 µmol of xylose per minute under the specified assay conditions (50 °C, pH 6.0) (Chen et al. 2016). The enzyme concentration in the crude extract was adjusted to ensure that the reaction remained within the linear range of the assay, typically using 0.1–0.5 U of enzyme per reaction. All assays were performed in triplicate to ensure reproducibility, and the results were averaged to determine the final xylanase activity. Bacterial biomass was harvested by centrifugation, freeze-dried, and weighed to determine the dry cell weight (mg/mL) for normalization of enzyme activity. The enzyme activity in units per gram of bacterial biomass (U/g) was calculated by first determining activity per milliliter of crude extract (U/mL) and then normalizing to the biomass concentration. Activity per milliliter was calculated using the following equation (Chen et al. 1986):

$$\mathrm{U/mL} = \frac{\mu mol\ xylose\ released\ \times\ dilution\ factor}{\text{reaction time (min) times:enzyme volume (mL)}}$$

To express xylanase activity relative to bacterial biomass, the U/mL value was divided by the concentration of biomass in the crude enzyme solution (mg/mL) and multiplied by 1000:

$$\mathrm{U/g} = \frac{\mathrm{U/mL}}{\text{mg biomass/mL enzyme solution}} \times\ 1000$$

Partial enzyme purification, sodium dodecyl sulfate-polyacrylamide gel electrophoresis (SDS-PAGE) and zymography

The xylanase enzyme was partially purified using ammonium sulfate precipitation on ice. Initially, 50 ml of bacterial culture supernatant was subjected to 100% ammonium sulfate saturation under constant stirring. After 2 h, the proteins were precipitated by centrifugation at 8000 rpm for 20 min at 4 °C, and then resuspended in 1 ml deionized water. To further purify the enzyme and remove any remaining ammonium sulfate, we used a dialysis bag. The concentrated enzyme solution was dialyzed against deionized water using a cellulose membrane with a 12–14 kDa MWCO (Sigma-Aldrich, #D9777) to remove residual ammonium sulfate and for further purification. The protein precipitation solutions were then used for SDS-PAGE and evaluated for enzymatic activity.

SDS-PAGE was conducted using a 12% gel, following the standard methods. In this regard, the gels were stained using Coomassie Brilliant Blue R-250 to visualize protein bands. Excess staining was removed through repeated washes with a destaining solution composed of methanol, glacial acetic acid, and distilled water in a 1:1:8 ratios by volume. The molecular mass of the purified xylanase was estimated by comparing its electrophoretic mobility to the relative mobility of a protein marker (BIO-RAD Precision Plus Protein Dual Color Standards, 500 µL #1610374).

Determining the optimal pH and temperature for xylanase activity

The impact of pH and temperature on xylanase activity was examined through a split-plot design experiment in triplicate, where partially purified enzymes were incubated in buffers with pH levels ranging from 3 to 10 for durations of 20, 40, and 60 min at temperatures of 40 and 50 °C. Notably, a broader temperature range was tested, from 20 °C to 90 °C. Briefly, 10 µL partially purified enzyme was added in a series of buffers tailored to specific pH ranges: 50 mM sodium citrate (pH 3.0–4.0), 50 mM sodium acetate (pH 4.0–5.5.0.5), 50 mM phosphate (pH 6.0–7.0), and 50 mM Tris-HCl (pH 7.5–9.0.5.0), with NaOH used to achieve a pH of 10 (Souza et al. 2012). Enzymatic activity was subsequently evaluated at three distinct time points to assess the effects of pH and temperature on xylanase activity. The collected data were analyzed using SAS software employing a two-factor split-plot design across time.

Kinetic analysis

Initial reaction velocities (V_0) were calculated from the amount of reducing sugar released during the incubation period, which corresponded to the linear phase of product formation. Reaction velocities were expressed as mg mL^{-1} min^{-1}. Michaelis–Menten kinetic parameters (Km and Vmax) were determined by nonlinear regression of the Michaelis–Menten equation. Lineweaver–Burk plots were constructed as a linear transformation to confirm the kinetic parameters. The turnover number (kcat) was calculated using the estimated Vmax values and the molar concentration of enzyme, assuming a molecular weight of 23 kDa. Catalytic efficiency was expressed as kcat/Km (Mittal et al. 2013).

Morphological and molecular characterization of the most potent isolates

To assess the morphological features of the screening samples and determine the purity of the isolated colonies, Gram staining was utilized. Molecular identification of the strains was performed using the sequences of the *rpoB* and *16 S* rRNA genes, followed by the construction of a phylogenetic tree. For this purpose, bacterial DNA was extracted using the CTAB 10% method (William et al. 2012). Polymerase chain reaction (PCR) was employed for amplification, using the primers 16sF (5'-AGAGTTTGATCCTGGCTCAG-3') and 16sR (5'-TACGGYTACCTTGTTTACGACTT-3'), as well as rpoBF (5'-AGGTCAACTAGGTTCAGTGAT-3') and rpoBR (5'-AAGAACCATAACCGGCAACTT-3'). The reaction mixture for the PCR amplification comprised 20 ng of DNA template, 0.5 µL of each primer (10 pmol), 1 µL of dNTPs (10 mM), and 0.5 units of Taq DNA polymerase, resulting in a total volume of 50 µL. The thermal cycling conditions were as follows: an initial denaturation step at 95 °C for 5 min, followed by 30 cycles consisting of denaturation at 95 °C for 30 s, annealing at 58 °C for 30 s, and extension at 72 °C for 1 min. A final extension step was conducted at 72 °C for 5 min to ensure complete amplification of the target fragment. The resulting PCR products were sequenced using the Sanger method by Novogene company. The obtained sequences were then analyzed using

the Sage tool from the gear-genomics server (Rausch et al. 2020) for quality control and editing. To determine the genus and species of the strains, initially a BLAST analysis was performed on the NCBI database to identify related genera. Subsequently, related *rpoB* and *16 S* sequences from 41 *Bacillus* spp. genomes were retrieved from NCBI database. Multiple sequence alignment was performed using Muscle software (Edgar 2004), and trimAL (Capella-Gutiérrez et al. 2009) was employed to remove weak regions of the multiple alignments. A phylogenetic tree was constructed using the GTRGAMMA model and bootstrap 100 in RaxML (Stamatakis et al. 2005). Finally, the phylogenetic tree was visualized using the iTOL online software (https://itol.embl.de/).

Whole genome sequencing

For genome sequencing, DNA was extracted from an overnight culture of strain S3 using the DNeasy UltraClean microbial kit (Qiagen LLC, Germantown, MD, USA) following the manufacturer's instructions. Strain S3 was selected for whole genome sequencing due to its higher xylanase activity, particularly at lower pH, which is of significant interest for this research. Subsequently, whole-genome library preparation (insert size: 360 bp) and sequencing were conducted by Novogene (UK) on the NovaSeq X Plus Series platform (PE150), yielding 1 Gb of sequencing data.

To ensure high data quality, the read quality was first evaluated using FastQC v0.11.2 (Brown et al. 2017). Following quality control, the de novo assembly of the genome was performed with SPAdes v3.12 (Bankevich et al. 2012; Prjibelski et al. 2020). The assembled scaffolds were then subjected to a BLAST analysis against all validly described *Bacillus* species ($n=123$) genomes to identify closely related species and infer the taxonomic position of strain S3 through phylogenetic relationships. Further comparative analysis was conducted using digital DNA-DNA hybridization (dDDH) and average nucleotide identity (ANI) values, which were calculated using the Genome-to-Genome Distance Calculation (GGDC 2.0, https://ggdc.dsmz.de) (Meier-Kolthoff et al. 2013), the orthoANI calculator on the EzTaxon-e server, and the ANIb tool on the JSpeciesWS web server (https://jspecies.ribohost.com/jspeciesws/#home). This combination of analyses provided robust insights into genomic similarity and taxonomic position.

To enhance assembly accuracy, scaffolds were rearranged using the CSAR-web tool (Chen and Lu 2018) and remaining gaps between scaffolds were filled using Figbird (Tarafder et al. 2022). The sequences were then used for reference to guide the scaffolding with *Bacillus subtilis* subsp *spizizenii* (ASM22746v1) by RagTag (Alonge et al. 2022). The finalized genome sequence data were subsequently uploaded to the Type (Strain) Genome Server (TYGS; https://tygs.dsmz.de), a platform designed for comprehens ive whole-genome-based taxonomic analysis. The genome was annotated through Prokka version 1.12 (Seemann 2014). Finally, to explore the potential for antimicrobial biosynthesis, antiSMASH v7.0 (Blin et al. 2019) was employed to identify secondary metabolite biosynthetic gene clusters and to compare these clusters with those in related genomes available in the NCBI database, focusing specifically on the complete and closed genome of strain.

Insilico analysis of xylanase gene

Following the annotation of xylanase genes, further characterization was undertaken to analyze their properties. The sequences of the xylanase genes, *xynA* and *xynB*, were initially assessed using the Compute pI/MW tool on the ExPASy server (https://web.expasy.org/compute_pi/) (Gasteiger et al. 2003) to determine physicochemical attributes, including the isoelectric point (pI) and molecular weight. Secondary structural features of the enzymes were predicted using GOR V server (https://npsa.lyon.inserm.fr/cgi-bin/npsa_automat.pl?page=/NPSA/npsa_gor4.html) (Sen et al. 2005).

Molecular docking

The three-dimensional structures of the three enzymes were generated using the AlphaFold2 tool (Jumper et al. 2021). Prior to modeling, the predicted N-terminal signal peptides were identified using SignalP 5 (Almagro Armenteros et al. 2019) and removed to generate models of the mature, secreted proteins. The quality and structural integrity of the resulting protein models were evaluated using the Ramachandran plot (Sheik et al. 2002), ERRAT analysis (Hasan et al. 2015), and Verify3D assessment (Eisenberg et al. 1997) using SAVES v6.1 (https://saves.mbi.ucla.edu/). After validation, the models were employed for molecular docking studies. A docking analysis was performed to examine the interaction dynamics between the three xylanase genes and ligand molecules. This study utilized AutoDock Vina 1.2.0 (Eberhardt et al. 2021) as the docking tool. Ligand structures were converted into the PDBQT format, which is the required input format for AutoDock Vina. The grid box centers and dimensions were determined using UCSF Chimera software (Pettersen et al. 2004). Binding energies of the docked complexes were calculated in kilocalories per mole. The resulting docked poses were visualized and analyzed in UCSF Chimera (Pettersen et al. 2004), and the molecular interactions were further explored using Discovery Studio (Biovia 2016).

Table 1 Sample types and corresponding regions for xylanase-producing strain isolation

Strains	Sample type	Province	City
S1	Spring water	Chaharmahal and Bakhtiari	Kuhrang
S3	Gavakhuni swamp soil	Isfahan	Varzane
S4	Desert soil	Isfahan	Kashan
S5	Forest soil	Mazandaran	Nowshahr
S6	Vinegar (20-year-old)	Isfahan	Kashan
S10	Sheep manure	Isfahan	Khomeini-shahr
S11	Sourdough	Isfahan	Khomeini-shahr
S12	Chicken intestine contents	Isfahan	Khomeini-shahr
S13	Chickpea field soil	Kurdistan	Qorveh
S14	Fish farming effluent	Ilam	Ilam
S16	Wheat field soil	Kurdistan	Qorveh
S17	Effluent of fermentation industries	Arak	Arak
S18	Si Sangan forest soil	Mazandaran	Nowshahr

Statistical analysis

Xylanase activity data were analyzed using a two-factor split-plot design with three independent replications ($n=3$). The whole-plot factor was temperature (two levels: 40 °C and 50 °C), and the sub-plot factors were strain (two levels: S3 and S4) and pH (six levels: 4, 5, 6, 7, 8, and 9). Time (three levels: 20, 40, and 60 min) was treated as a repeated measure. All factors were considered fixed effects. Analysis of variance (ANOVA) was performed using R software (version 4.2) with the aov() function. The lme4 package was used for mixed-effects modeling to account for the split-plot structure. Means were compared using Fisher's Least Significant Difference (LSD) post-hoc test at a significance threshold of $\alpha=0.05$. A significance level of $p<0.01$ was considered highly significant, and $p<0.10$ was considered marginally significant for time-related interactions.

Results

Isolation and identification of xylanase producer bacteria

All bacterial strains from the collected samples underwent an initial qualitative screening to assess xylanase activity. In this preliminary assessment, isolates were ranked by their PI, which ranged from 1.00 to 4.1 among the 18 isolates. Notably, isolates S3, S4, S5, S13, S14, and S16 exhibited high xylanase activity, forming prominent clear zones on the xylan medium. Isolates with a PI exceeding 1.5 were subsequently selected for quantitative analysis of xylanase production (Table 1).

In the subsequent quantitative analysis, each isolate was cultured in LB medium, and then xylanase activity was assessed using a standardized xylanase activity assay. Results indicated that enzyme activity peaked at 24 h' post-cultivation, exceeding activity levels observed at 48 and 72 h (Fig. 1). Among the isolates, strains S3 and S4 exhibited the highest xylanase activity, thus identifying them as the most effective enzyme-producing strains.

The highest absorbance values at 540 nm were 0.726 for S3 and 0.658 for S4. The crude, freeze-dried enzyme solutions had concentrations of 0.33 mg/mL for S3 and 0.29 mg/mL for S4. Based on the standard xylose curve, the xylanase activity was estimated as 11 U/mL for S3 and 10 U/mL for S4, corresponding to 34,480 U/g and 33,340 U/g, respectively. These results indicate that both strains produced high

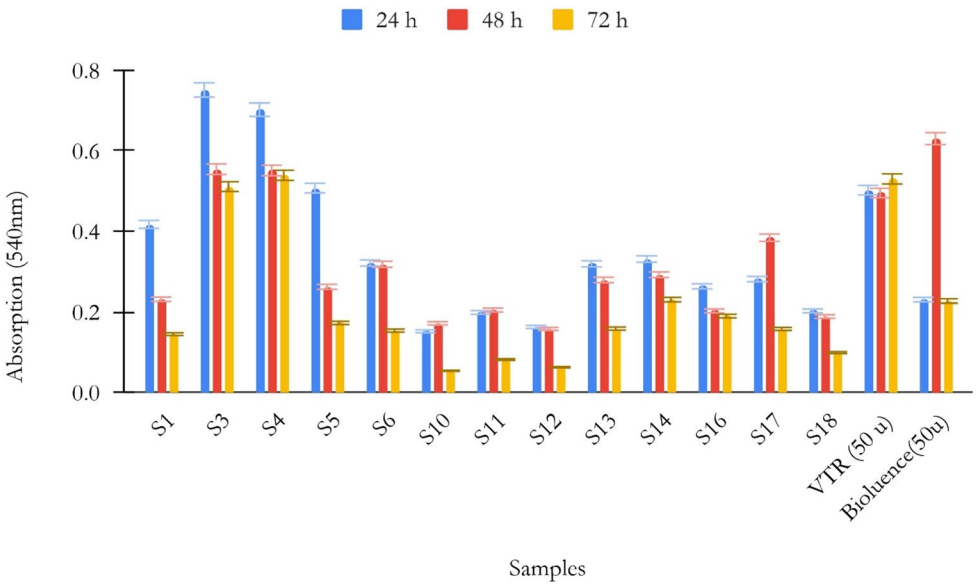

Fig. 1 Quantitative analysis of xylanase activity in isolates cultured in LB medium at three time points (24, 48, and 72 h). Data are presented as mean ± SEM. Error bars represent standard error of the mean

levels of xylanase, with S3 showing slightly higher activity than S4.

Enzyme purification and molecular weight

The xylanase enzyme was purified using ammonium sulfate precipitation. SDS-PAGE analysis revealed a distinct band at approximately 22 and 25 kDa (Fig S1), identifying this as the estimated size of the xylanases produced by strains S3 and S4.

Identifying optimal pH and temperature for activity

The stability and functionality of xylanase enzymes were examined under varying temperature and pH conditions using a two-factor split-plot design over time, conducted at 40 °C and 50 °C with three replications. Strains S3 and S4 were selected for this experiment due to their superior xylanase activity in preliminary assessments. The comparative pH-activity profiles revealed distinct enzymatic adaptations between the strains (Fig. 2). The analysis of variance demonstrated highly significant effects ($p < 0.01$) for strain, pH, and their interactions on xylanase activity, with time interactions also significant at $p < 0.10$ (Table S1−10). At 40 °C, the S3 strain showed the highest activity at pH 9 (11.56 U/mL) and maintained stable performance across a broad pH range (4–9), highlighting its versatility for processes requiring pH adaptability. In contrast, the S4 strain exhibited optimal activity at neutral pH (8.67 U/mL at pH 7) but demonstrated marked sensitivity to acidic conditions (1.89 U/mL at pH 4). At 50 °C (Fig. 2), the S4 strain outperformed S3 in thermal stability and activity, achieving peak performance at pH 9 (9.35 U/mL). Strain S3 maintained robust activity across pH 6–9 but showed reduced functionality under acidic conditions at this elevated temperature. The commercial VTR xylanase displayed consistent but moderate activity across both temperatures, with optimal performance at alkaline pH. Temporal analysis further revealed that at 50 °C, the S4 strain reached its peak activity after 40 min (7.44 U/mL), demonstrating robust heat tolerance under prolonged exposure to elevated temperatures. Overall, these results delineate complementary industrial potentials: S3 strain is optimal for applications requiring pH resilience across a wide range, while the S4 strain is better suited for high-temperature, alkaline processes. This functional divergence underscores the value of strain-specific selection for tailored industrial applications.

Xylanase activity and Michaelis–Menten kinetics

Both xylanases from bacterial strains S3 and S4 exhibited typical Michaelis–Menten kinetics across the tested

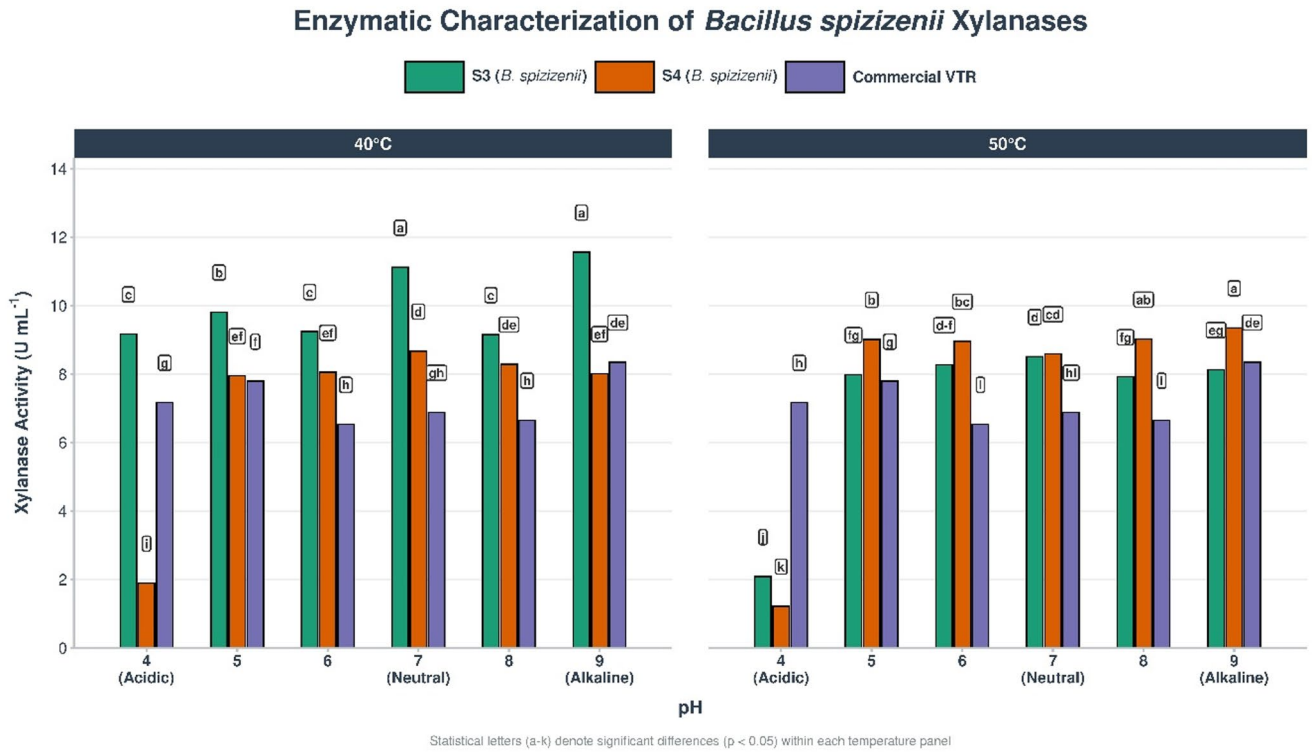

Fig. 2 PH-activity profiles of xylanases from *B. spizizenii* strains S3, S4, and commercial VTR at 40 °C and 50 °C. Activity (U/mL) was measured across pH 4–9. Different lowercase letters above bars indicate statistically significant differences within each temperature panel ($p < 0.05$, LSD test). Letters correspond to those in Supplementary Tables

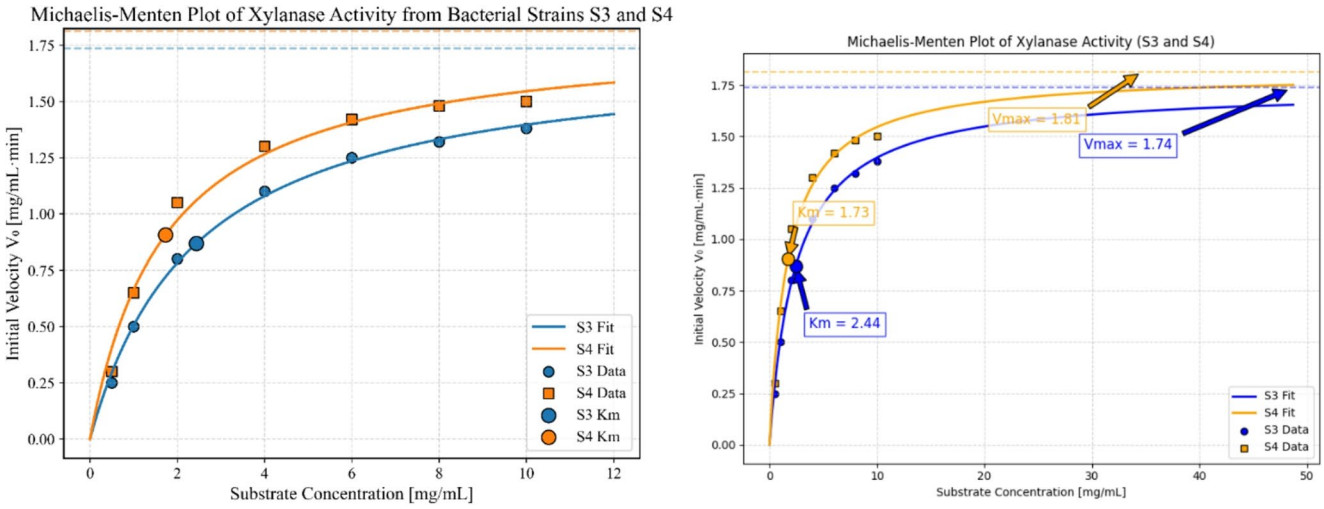

Fig. 3 Michaelis–Menten plots of xylanase activity from strains S3 and S4 under optimal conditions (pH 7.0, 50 °C). Experimental data points are shown, fitted curves represent Michaelis–Menten regression, horizontal dashed lines indicate Vmax, and large points mark Km values

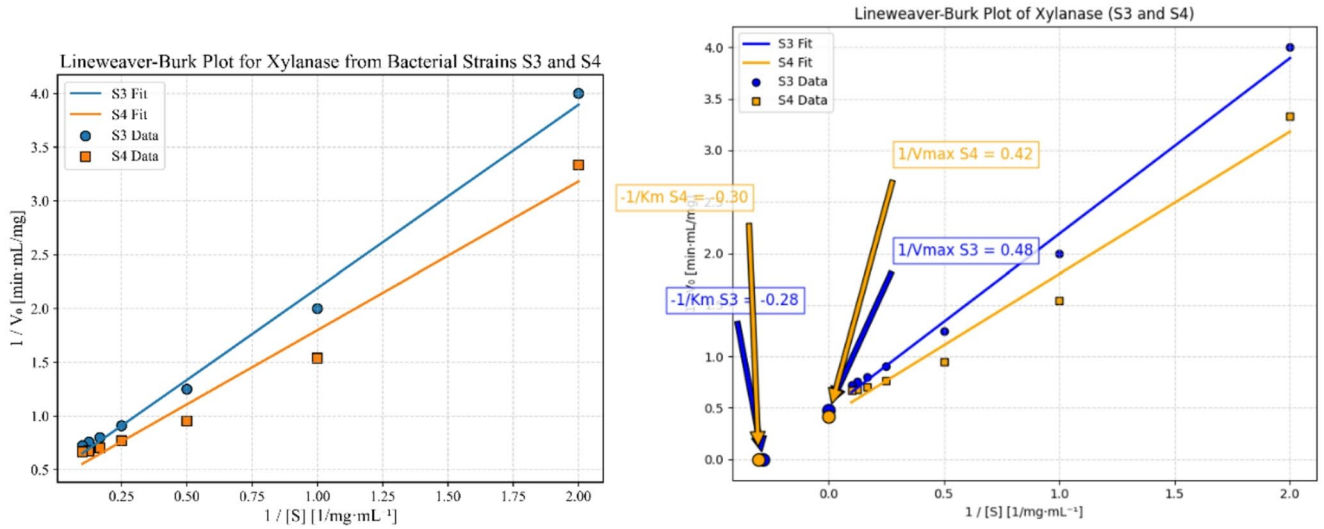

Fig. 4 Lineweaver–Burk plots used to verify kinetic parameters of xylanases from strains S3 and S4

substrate concentrations (0.5–10 mg·mL⁻¹). Increasing the substrate concentration resulted in a corresponding increase in the initial reaction velocity (V_0) until a saturation plateau was reached (Fig. 3). The xylanase from strain S4 displayed a slightly higher maximum reaction rate (Vmax = 1.50 mg·mL⁻¹·min⁻¹) compared to strain S3 (Vmax = 1.40 mg·mL⁻¹·min⁻¹). Moreover, the apparent Michaelis constant (Km) of S4 (1.2 mg·mL⁻¹) was lower than that of S3 (2.2 mg·mL⁻¹), indicating a higher substrate affinity for the S4 enzyme. Lineweaver–Burk plots (Fig. 4) confirmed the kinetic parameters obtained from nonlinear regression. The xylanase from S4 exhibited a lower slope and smaller y-intercept than S3, consistent with its higher Vmax and lower Km values. In the Michaelis–Menten plots (Fig. 3), the points indicate experimental data, the fitted lines represent the nonlinear regression, the horizontal dashed lines show Vmax, and the large points indicate Km values (where V_0 = Vmax/2).

Catalytic efficiency

The turnover number (kcat) of S4 xylanase (357 min⁻¹) was higher than that of S3 (293 min⁻¹). Consequently, the catalytic efficiency (kcat/Km) of S4 was approximately 2.2-fold higher than that of S3, indicating superior substrate utilization and overall catalytic performance.

Morphological and molecular characterization of the most potent isolates

Morphological evaluation of the colonies revealed distinct characteristics for the S3 and S4 strains. The S3 strain exhibited irregularly shaped colonies with a creamy coloration and curled margins, while the elevation of these colonies was flat. In contrast, the S4 strain formed circular colonies that were also cream-colored but featured a darker central region. The margins of the S4 colonies were entire, and their elevation was similarly flat, presenting a smooth and uniform appearance. To further assess the morphological characteristics of the isolated bacteria and ensure the purity of the colonies, Gram staining was performed. Microscopic examination indicated that both screening strains were Gram-positive and rod-shaped. The Gram-positive bacteria displayed a thick peptidoglycan layer and reduced lipid content in their membranes, resulting in a purple coloration under the microscope. For molecular identification of isolated strains, fragments of the *rpoB* and *16 S rRNA* genes were sequenced and subjected to BLAST analysis against the NCBI nucleotide database. We selected the *rpoB* gene in conjunction with the *16 S* rRNA gene for the identification of *Bacillus* strains due to the enhanced resolution it provides for species differentiation. The *rpoB* gene encodes the beta subunit of RNA polymerase and exhibits significant polymorphism among *Bacillus* species, which allows for more precise identification than the *16 S* rRNA gene alone. The *16 S* rRNA gene, while widely used, can have limited resolution at the species level due to its conserved nature. Additionally, the *rpoB* gene is a single-copy gene, making it a reliable alternative for taxonomic studies in microbial ecology. By employing both genes, we increase the reliability and accuracy of strain identification, which is crucial for understanding the ecological roles and potential applications of these Bacillus strains in various biotechnological contexts (Case et al. 2007; Ogier et al. 2019). The results demonstrated a high degree of similarity to species within the *Bacillus* genus. For further phylogenetic analysis, the complete genome sequences of *Bacillus* species were

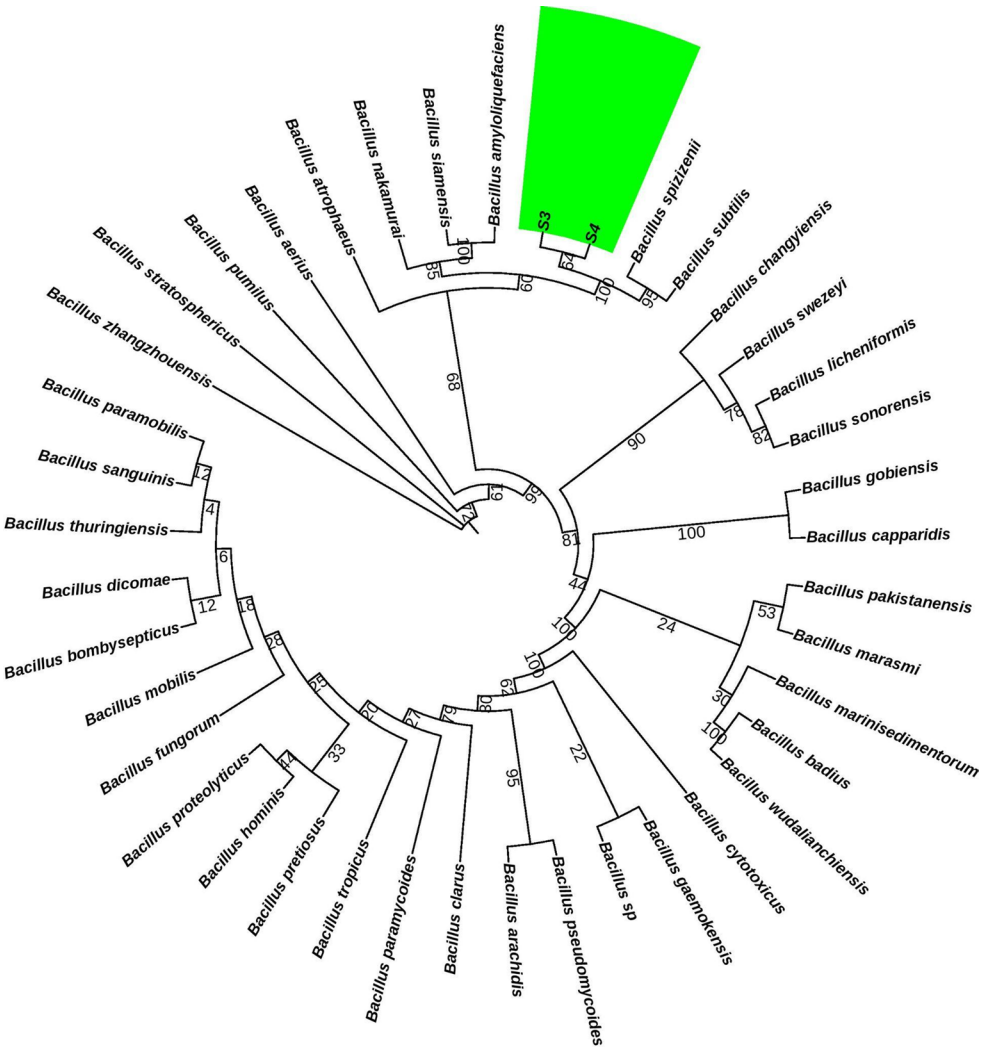

Fig. 5 Maximum likelihood phylogenetic tree generated from concatenated *rpoB* and 16 S rRNA gene sequences of 40 *Bacillus* species, illustrating the genetic relationships between strains S3, S4, and *Bacillus spizizenii*. The tree was constructed using RAxML with the GTRGAMMA model. Bootstrap values (100 replicates) are shown at each node. The scale bar represents the number of substitutions per site. Strains S3 and S4 are highlighted in bold

Table 2 Summary of genome assembly and refinement using SPAdes, CSAR, Figbird, and Pilon+Ragtag tools

	SPAdes	CSAR	Figbird	pilon+ragtag
Genome (bp)	4,069,232	4,073,332	4,086,964	4,089,140
Contigs	71	30	28	27
N50 (bp)	501,746	2,946,046	2,959,912	4,033,705

Table 3 Comparative genomic analysis of *Bacillus* strains, including dDDH values, G+C content differences, gene number differences, and genome sizes

Subject strain	dDDH (d6, in %)	G+C content difference (in %)	gene number difference	genome size (Mb)
Bacillus spizizenii TU-B-10	96.5	0.05	248	4.2
Bacillus rugosus	81.8	0.76	155	4.1
Bacillus inaquosorum KCTC 13,429	82	0.19	331	4.3
Bacillus cabrialesii TE3	82.6	0.24	165	4.1
Bacillus cabrialesii subsp. tritici TSO2	81.6	0.14	358	4.3
Bacillus subtilis ATCC 6051	79.3	0.36	375	4.2
Micromonospora provocatoris MT25	13.4	27.96	2588	6
Bacillus stercoris D7XPN1	80.1	0.08	366	4.3
Bacillus vallismortis DV1-F-3	64.7	0.11	62	3.9
Bacillus tequilensis NCTC13306	63.2	0.1	193	4
Bacillus mexicanus FSQ1	65.5	0.91	−211	3.6
Bacillus axarquiensis NRRL B-41,617	70.9	0.08	574	4.6

retrieved. Using the Linux command line, the corresponding *rpoB* and *16 S* gene fragments were isolated from 41 species. After sequence alignment, editing, and matrix construction, a phylogenetic tree was generated using RAxML software (Fig. 5). The resulting phylogenetic tree indicated that the S3 and S4 strains are likely the same species as *B. spizizenii*,

Genome sequence and characterization of xylanase genes

Genome sequencing generated approximately 9.086 million paired-end reads, providing ~ 0.9 Gb of data with an average coverage depth of ~ 150×. The initial assembly using SPAdes produced a genome of 4,069,232 bp, distributed across 71 contigs, with an N50 value of 501,746 bp (Table 2). Subsequent refinement with CSAR improved the assembly, reducing the number of contigs to 30, increasing the genome size to 4,073,332 bp, and enhancing the N50 to 2,946,046 bp. Gap filling with Figbird further improved the assembly, yielding 28 contigs with a genome size of 4,086,964 bp and an N50 of 2,959,912 bp. Final scaffolding and polishing using Pilon and Ragtag resulted in a high-quality assembly comprising 27 contigs, a total genome size of 4,089,140 bp, and an N50 value of 4,033,705 bp.

The ANI analysis between the assembled genome and *B. spizizenii* revealed a high degree of genomic similarity, with an ANI value of 99.07%, corresponding to 94.71% of aligned bases. The DDH estimate, calculated using the GLM-based method, was 93.10%, indicating a very close relationship between the two genomes. The probability that the DDH value exceeds 70%, suggesting that the strains belong to the same species, was 96.72%, based on logistic regression analysis. These results collectively support the taxonomic proximity of the assembled genome to *B. spizizenii*, reinforcing its identification within this species. Comparison of the genome of strain S3 with other *Bacillus* strains revealed significant differences in dDDH values (Table 3). The dDDH values for *B. spizizenii* strains ranged from 81.6% to 96.5%, indicating varying degrees of genetic relatedness among them. In contrast, comparisons with *Bacillus subtilis* showed a dDDH value of 79.3%, suggesting a greater genetic divergence between these species. Other strains, such as *Bacillus rugosus* and *Bacillus inaquosorum*,exhibited dDDH values of 81.8% and 82.0%, respectively, further highlighting the genetic diversity within the *Bacillus* genus. The comparison of genome sizes among the *Bacillus* strains revealed notable differences that had implications for their genetic content and functional capabilities (Table 3). Strain S3, with a genome size of 4.09 Mb, was comparable to other *B. spizizenii* strains, which generally exhibited similar genome sizes. In contrast, *Bacillus subtilis* had a slightly larger genome size of 4.2 Mb, while other strains such as *Bacillus inaquosorum* and *Bacillus cabrialesii* subsp. tritici showed genome sizes of 4.3 Mb. The presence of gaps in the genome of strain S3 may have limited the identification of certain genes and functional elements, potentially impacting the understanding of its metabolic capabilities.

The phylogenetic tree generated by TYGS analysis illustrated the evolutionary relationships between strain sequenced in this study (S3) and other closely related *Bacillus* species (Fig. 6). The tree showed that our strain was most closely related to *B. spizizenii* TU-B-10. These strains formed a tightly-knit clade, indicating high genomic similarity. Further analysis placed *Bacillus inaquosorum* KCTC 13,429 and *Bacillus vallismortis* DV1-F-3 within a slightly more distant branch. This suggested a lower but still significant genomic affinity. In contrast, *B. subtilis* strains (ATCC 6051 and NCIB 3610), along with *Micromonospora provocatoris* MT25 and *Bacillus stercoris* D7XPN1, were

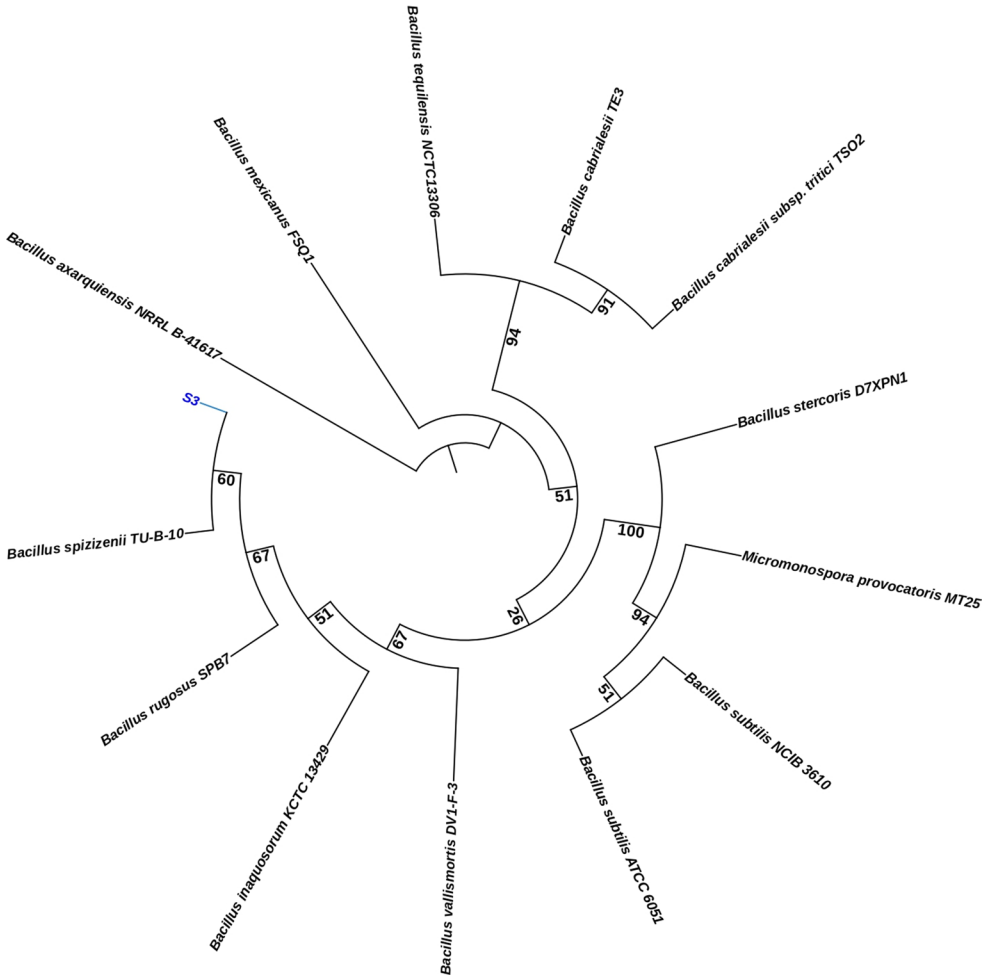

Fig. 6 Whole-genome-based phylogenetic tree illustrating the evolutionary relationships of strain S3 with closely related Bacillus species. The tree was generated using the Type (Strain) Genome Server (TYGS). Bootstrap support values (based on 100 replicates) are indicated at the branch points. The scale bar represents the estimated evolutionary distance (genome BLAST distance phylogeny, GBDP)

placed in more distant branches with higher divergence values, indicating these species were not as closely related to our strain. Additional branches included *Bacillus cabrialesii* subsp. *tritici* TSO2, *Bacillus tequilensis* NCTC13306, and other *Bacillus* species such as *Bacillus mexicanus* FSQ1 and *Bacillus axarquiensis* NRRL B-41,617, with increasing branch lengths suggesting progressively greater evolutionary distances from our strain.

Through the genome annotation analysis, the S3 genome was predicted to contain 4,056 coding sequences (CDSs), all of which were functionally annotated. The comparison of gene numbers among the *Bacillus* strains revealed significant differences that may have also implications for their genetic content and functional capabilities. Strain S3 exhibited a gene number difference of 248 genes when compared to other *B. spizizenii* strains, indicating a unique genetic makeup. In contrast, *Bacillus subtilis* showed a gene number difference of 375 genes, suggesting a more extensive genetic divergence between this species and strain S3. Other strains, such as *Bacillus rugosus* and *Bacillus inaquosorum*, exhibited gene number differences of 155 and 331 genes, respectively, further highlighting the genetic diversity within the *Bacillus* genus (Table 3). Additionally, the S3 genome includes 8 ribosomal RNA (rRNA) and 99 transfer RNA (tRNA) genes.

AntiSMASH analysis revealed that the S3 genome harbors genes encoding novel secondary metabolites with antimicrobial properties. Specifically, six gene clusters encoding non-ribosomal peptide synthetases (NRPS), one cluster for Type III polyketide synthase (T3PKS), one cluster for cyclodipeptide synthetase (CDPS), one cluster for sactipeptide biosynthesis, four clusters for lanthipeptides (ribosomally synthesized and post-translationally modified peptides, RiPPs), and two clusters for bacilysin biosynthesis were identified in the S3 genome. Among the four gene clusters encoding NRPS, five clusters exhibited 100% similarity to genes involved in the biosynthesis of bacillibactin, paenibactin, bacillaine, mycosubtilin, and surfactin. One additional cluster displayed 70% similarity to gene clusters associated with bacillibactin biosynthesis (Fig. 7).

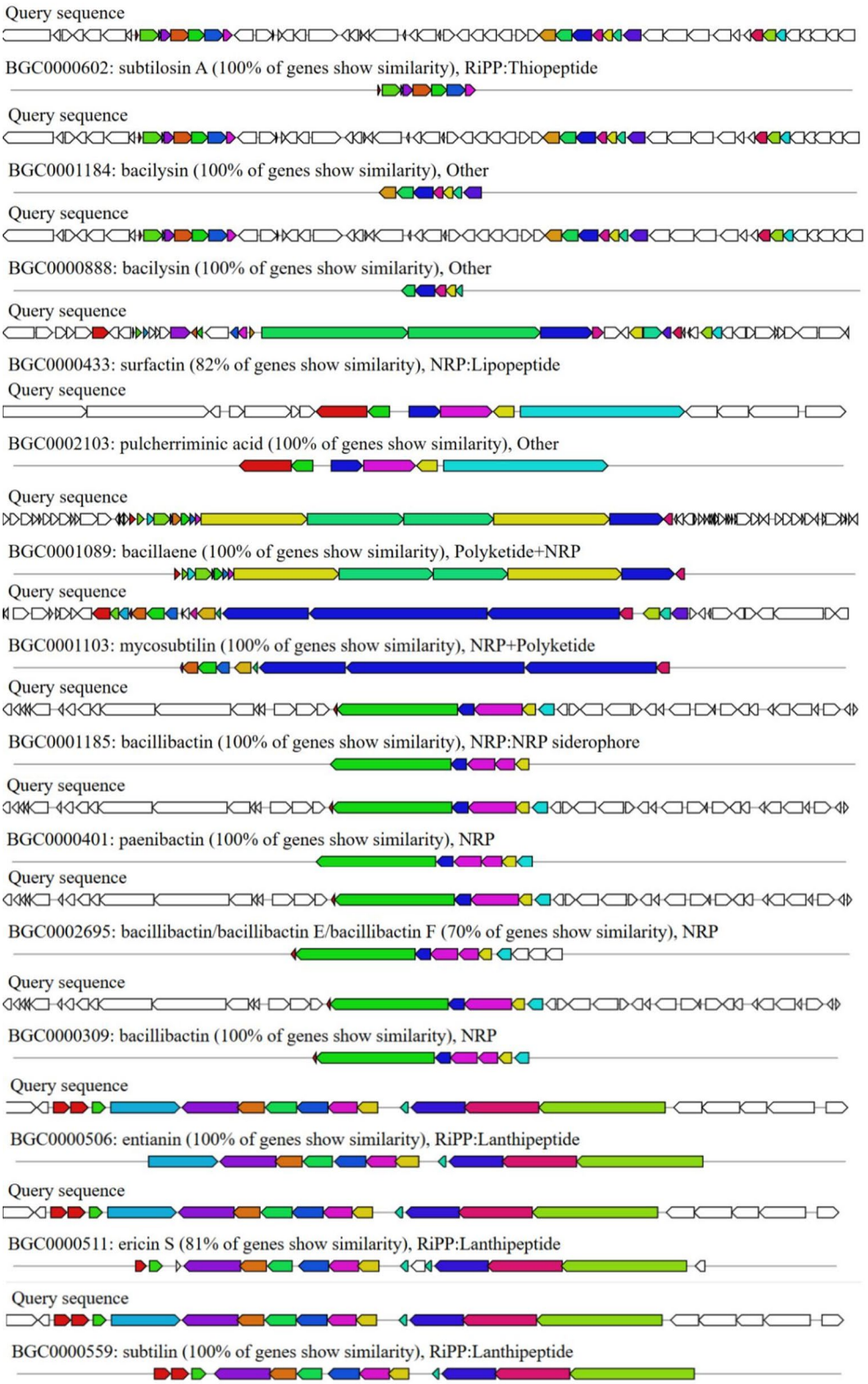

Fig. 7 Schematic representation of putative biosynthetic gene clusters (BGCs) identified in the genome of *B. spizizenii* S3 using antiSMASH v7.0. Each colored arrow represents a gene within a BGC. Colors indicate different BGC types. Percentages indicate the similarity (%) of each cluster to known BGCs in the MIBiG database

In silico analysis

To identify potential target enzyme genes, three xylanase genes were characterized: one *xynB* gene (1602 bp), showing 98% sequence similarity to the reference genome of *B. spizizenii*, and two *xynA* genes (*xynA1*: 699 bp and *xynA2*: 642 bp). BLASTx homology search against the UniProt database and sequence similarity search against RCSB Protein Data Bank classified *xynA* and *xynB* genes as members of the GH11 and GH43 xylanase families, respectively. The physicochemical and structural characterization of the xylanase proteins revealed distinct variations in their properties (Table 4). The isoelectric point (pI) ranged from 5.82, observed in *xynB*, to 9.32 in *xynA1*. The molecular weight values spanned from 23.31 kDa for *xynA2* (the lowest) to 61.36 kDa for *xynB*.Regarding secondary structure composition, the alpha-helix content varied between 7.51% for *xynA2* and 23.45% for *xynB*). The percentage of extended strand ranged from 23.26% in *xynB* to 44.13% in *xynA2*. Additionally, the random coil content showed a variation from 48.36% in *xynA2* to 53.28% in *xynB*.

Molecular docking

The quality assessment of the protein models demonstrated robust structural accuracy. Ramachandran plot analysis revealed that 86.96% of residues for *xynA1*, 91% for *xynA2*, and 95.48% for *xynB* were located within the core region, indicating high stereochemical quality. Additionally, the ERRAT scores for the modeled proteins were 82.30 for *xynA1*, 83.60 for *xynA2*, and 85.65 for *xynB*, further supporting the structural reliability and accuracy of the models. The docking analysis of three xylanase enzymes (*xynA1*, *xynA2*, and *xynB*) with three ligands (xylan, α-D-xylopyranose, and β-D-xylopyranose) revealed distinct binding affinities and interaction patterns (Table 5). Among the three enzymes, *xynA1* exhibited the strongest affinity with xylan (−9.4 kcal/mol), mediated by interactions with Glu45, Arg76, Pro159, Glu121, and Tyr203, while its affinities for α-D-xylopyranose and β-D-xylopyranose were moderate (−5.5 and −5.4 kcal/mol, respectively), involving residues such as Asn72, Tyr123, Gln169, and Arg155.

Table 4 Physicochemical and secondary structural properties of xylanase enzymes identified in *B. spizizenii* S3

Xylanase (Family)	Isoelectric point (pI)	Molecular weight (kDa)	Alpha-helix (%)	Extended strand (%)	Random coil (%)
xynA1	9.32	25.72	10.78	37.07	52.16
xynA2	9.20	23.30	7.51	44.13	48.36
xynB	5.82	61.36	23.45	23.26	53.28

Table 5 Binding energy and functional residues of docking between the different xylanase genes from *B. spizizenii* S3 (*xynA1*, *xynA2*, and *xynB*) and ligands (xylan, α-D-xylopyranose, and β-D-xylopyranose)

Receptor	Ligand	Affinity (kcal/mol)	Interacting amino acid
xynA1	Xylan	−9.4	Glu45, Arg76, Pro159, Glu121, Tyr203
	a-D-xylopyranose	−5.5	Asn72, Glu210, Tyr123, Gln169, Arg155
	b-D-xylopyranose	−5.4	Tyr123, Pro159, Gln169, Arg155, Glu121
xynA2	Xylan	−8.1	Thr90, Arg111, Gln126, Glu171
	a-D-xylopyranose	−5.5	Gln6, Tyr68, Pro115
	b-D-xylopyranose	−5.2	Asn34, Pro115, Glu171
xynB	Xylan	−8.2	Cys18, Arg19, Cys76, Ser80, Asp133, Thr134, His189, Leu190
	a-D-xylopyranose	−5.6	Ile17, Phe131, Leu190
	b-D-xylopyranose	−5.4	Leu130, His189

This computational predictions i supported by kinetic analysis. Similarly, *xynA2* demonstrated a notable binding affinity with xylan (−8.1 kcal/mol), interacting with Thr90, Arg111, Gln126, and Glu171 (Fig. 8), whereas its interactions with α-D-xylopyranose and β-D-xylopyranose (−5.5 and −5.2 kcal/mol, respectively) involved Gln6, Pro115, and Glu171. For *xynB*, the binding affinity with xylan (−8.2 kcal/mol) was supported by extensive interactions with Cys18, Arg19, Ser80, Asp133, and His189, while the affinities for α-D-xylopyranose (−5.6 kcal/mol) and β-D-xylopyranose (−5.4 kcal/mol) involved fewer residues, such as Ile17, Phe131, Leu130, and His189.

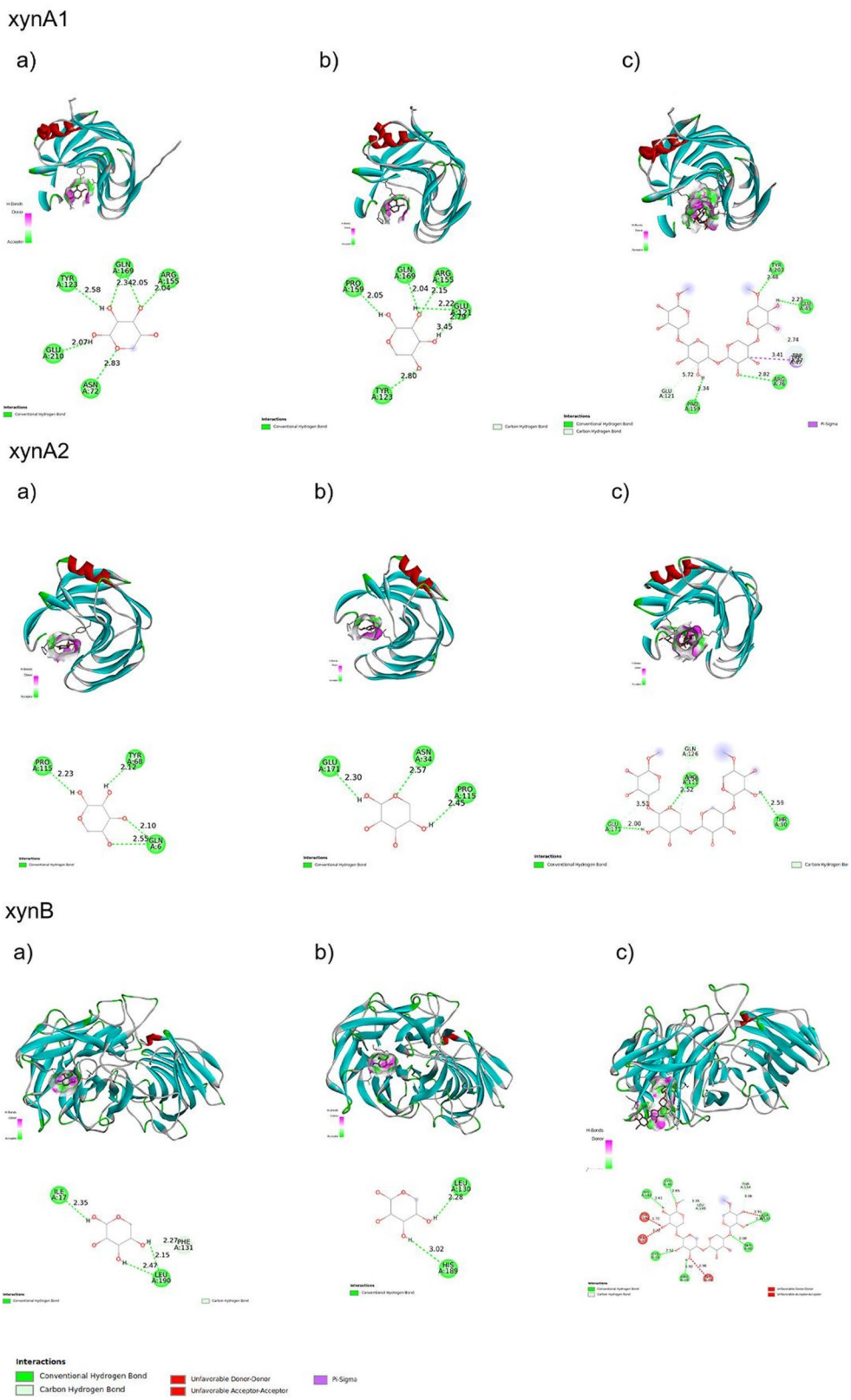

Fig. 8 Molecular interaction of three xylanase genes identified in *B. spizizenii S3* (*xynA1*, *xynA2*, and *xynB*) and ligands (xylan, α-D-xylopyranose, and β-D-xylopyranose). The detailed view of the binding site with substrate and amino acids involved in interaction and making hydrogen bonds

Discussion

The continuous search for new xylanase-producing bacterial strains with desirable enzymatic properties is crucial for advancing industrial applications, particularly in sectors such as biofuels, food processing, and paper manufacturing. In this study, we successfully isolated and characterized xylanase-producing strains from diverse environmental samples in Iran, with a particular focus on strains S3 and S4, which exhibited exceptional xylanase activity. The findings highlight the potential of these strains as valuable resources for industrial enzyme production, particularly given their ability to function under broad pH and high temperature conditions.

The xylanases produced by strains S3 and S4 demonstrated optimal activity at alkaline pH levels (pH 9) and elevated temperatures (40 °C for S3 and 50 °C for S4). Notably, strain S3 exhibited activity across a broad pH range, maintaining significant enzymatic function from pH 4 to pH 9, which is a remarkable characteristic not commonly observed in xylanases derived from other bacterial sources. This broad pH tolerance is particularly significant, as many industrial processes operate under varying pH conditions, where traditional xylanases often exhibit reduced activity and stability. Previous research has shown that bacterial xylanases typically exhibit optimal activity in acidic to neutral pH environments, typically between pH 5 and pH 9. Some strains have shown optimal activity in alkaline conditions, particularly those from alkaliphilic sources, with some reaching optimal activity around pH 9. For instance, xylanases from *B. pumilus* SV-205 demonstrated optimal activity at pH 10.0 (Nagar et al. 2012), indicating a preference for alkaline conditions. In contrast, *B. subtilis* BS05 operated optimally at a more acidic pH of 5.0 (Irfan et al. 2011), suggesting its suitability for applications in environments with lower pH levels. Additionally, *Paenibacillus macerans* IIPSP3 was reported to have optimal activity at pH 4.5 (Dheeran et al. 2012), further emphasizing the diversity of pH preferences among xylanases. On the other hand, *Anoxybacillus flavithermus* WL showed optimal activity at neutral pH 7.0 (Ellis and Magnuson 2012), which may have been advantageous for processes that required a balanced pH. Moreover, *Gracilibacillus* sp. TSCPVG exhibited optimal xylanase activity at pH 7.5 (Poosarla and Chandra 2014), while *Kluyvera* sp. OM3 functioned best at pH 8.0 (Xin and He 2013). In contrast, fungal xylanases are predominantly characterized by their optimal activity in acidic conditions, typically ranging from pH 4.0 to pH 6.0. For example, *Aspergillus niger* has been shown to exhibit optimal xylanase activity at pH 7.5, indicating a slight preference for neutral conditions (Ahmad and Butt 2013). However, *Fusarium oxysporum* showed optimal performance at pH 6.0 (Christakopoulos et al. 1996). *Myceliophthora* sp. has been reported to have optimal xylanase activity at pH 6.0 and a temperature of 75 °C (Chadha et al. 2004). *Thermoascus aurantiacus* has been found to perform optimally at a pH range of 4.0 to 5.0 (Kalogeris et al. 1998). Moreover, *Geobacillus stearothermophilus* has been characterized by optimal xylanase activity at pH 6.0 and a temperature of 60 °C (Bibi et al. 2014). *Paenibacillus terrae* HPL-003 showed a remarkable adaptability, with an optimal pH range of 4–11 (Song et al. 2014). Furthermore, Liu et al. (2012) highlighted the stability of xylanases from various fungal sources, noting that many exhibit optimal activity around pH 6.0 (Liu et al. 2012). Accordingly, the exceptional properties of strain S3, particularly its broad pH tolerance and optimal activity at alkaline conditions, position it as a highly advantageous candidate for industrial applications, potentially enhancing the efficiency and versatility of xylanase utilization across various sectors.

In terms of temperature tolerance, bacterial xylanases often exhibit a broader range of thermal stability compared with their fungal counterparts. For example, xylanases from *Caldicoprobacter algeriensis* have been shown to retain activity at temperatures up to 80 °C (Mhiri et al. 2020), while fungal xylanases typically have lower thermal stability, with optimal activity generally observed within the range of 60 °C and 85 °C (Zhao et al. 2013; García-Huante et al. 2017). Research has demonstrated that the thermostability of xylanases is crucial for industrial applications, where high temperatures are used for the hydrolysis of hemicellulose (Bhardwaj et al. 2019). For instance, xylanases from thermophilic bacteria like *Geobacillus* sp. have shown remarkable stability, with half-lives of up to 18 days at 60 °C (Bhalla et al. 2015). In contrast, many fungal xylanases, while effective, often experience a significant loss of activity at elevated temperatures, limiting their application in high-temperature processes. Moreover, the ability of bacterial xylanases to function effectively at higher temperatures can lead to increased efficiency in enzymatic reactions, reducing the need for prolonged reaction times and minimizing the risk of microbial contamination (Yang et al. 2020a, b). The elevated temperature tolerance of strain S4, which exhibits optimal activity at 50 °C, aligns with these findings and suggests that these enzymes could be particularly useful in processes such as biomass conversion, biofuel production, and animal feed, where higher temperatures are often employed to enhance reaction rates.

Molecular and phylogenetic analyses revealed that strain S3 is a novel xylanase-producing variant of *B. spizizenii* from Iran, which has not been previously documented in the region based on available literature. The whole-genome sequencing of strain S3 identified unique xylanase genes belonging to the GH11 and GH43 families, which are

well-documented for their roles in xylan degradation (Paës et al. 2012; Takita et al. 2019; Zhang et al. 2021). The molecular weight of the xylanase produced by strains S3 and S4 was estimated to be approximately 22 kDa, which is consistent with the range reported for other bacterial xylanases (Jalal et al. 2009; Chakdar et al. 2016; Zarafeta et al. 2020) The structural characteristics of these enzymes, including the presence of a signal peptide at the N-terminus, indicating their suitability for secretion and potential biotechnological applications. The physicochemical properties, such as the isoelectric point and the ratio of positively to negatively charged residues, suggest that the xylanases from these strains are alkaline, consistent with the observed optimal activity at alkaline pH levels. This aligns with findings from other studies showing that the ratio of charged residues significantly influences the pH stability and activity of enzymes (Mamo et al. 2009; Wu et al. 2020; Dhaver et al. 2022).

Molecular docking studies have provided valuable insights into the interaction dynamics between the xylanases from *B. spizizenii* S3 and their substrates, revealing favorable substrate-binding capabilities that are essential for catalytic efficiency. The binding affinities observed, particularly for xynA1 with xylan (−9.4 kcal/mol), indicate a robust interaction facilitated by key amino acids such as Glu45, Arg76, and Tyr203. These residues are critical for stabilizing the enzyme-substrate complex, which is consistent with findings from other studies that emphasize the role of specific conserved residues in determining substrate specificity and catalytic performance across different xylanase families (Yang and Han 2018; Saleem et al. 2021; Dodda et al. 2021; Zheng et al. 2022). The moderate binding affinities for α-D-xylopyranose (−5.5 kcal/mol) and β-D-xylopyranose (−5.4 kcal/mol) further suggest that while these enzymes are optimized for larger substrates like xylan, they retain the ability to interact with smaller oligosaccharides, albeit with reduced efficiency (Putra et al. 2024). This observation aligns with the structural characteristics of other glycoside hydrolases, where substrate size significantly influences binding affinity and catalytic activity (Xiong et al. 2020; Li et al. 2022). The distinct interaction patterns among the three xylanases also highlight their functional diversity. For instance, *xynA2* and *xynB* exhibited binding affinities of −8.1 and −8.2 kcal/mol for xylan, respectively, with unique sets of interacting residues such as Thr90 and Cys18, which may confer different substrate preferences and catalytic mechanisms. The presence of these specific residues suggests that each enzyme may have evolved to fulfill particular roles in the degradation of hemicellulosic biomass. Furthermore, the high stereochemical quality of the modeled proteins, as indicated by the Ramachandran plot analysis and ERRAT scores, reinforces the reliability of these findings and supports the potential for enzyme engineering efforts aimed at enhancing stability and activity. By targeting the key residues identified in this study, researchers can design more efficient biocatalysts tailored for specific applications, thereby advancing the field of biotechnology and sustainable energy production. Overall, these findings underscore the significance of molecular docking as a powerful tool for elucidating the complexities of enzyme-substrate interactions and guiding future research in enzyme optimization.

Conclusion and recommendations

This study represents the first identification and comprehensive characterization of *B. spizizenii* from Iranian soil. The isolated strain demonstrated a robust ability to produce xylanase under broad pH adaptability, achieving a significant enzymatic yield of 11.56 U/mL under optimized conditions. Detailed biochemical analysis revealed that the enzyme operates efficiently across a broad pH and temperature range, highlighting its industrial applicability. Genome sequencing and molecular docking analyses highlighted the distinctiveness of the strain, shedding light on its genetic composition and the structural interactions of its xylanase enzyme with substrates. These computational findings are supported by kinetic analysis, although further experimental validation through mutagenesis is required to confirm the functional role of specific residues. The findings emphasize the potential of this strain for industrial-scale applications, particularly in the paper, textile, and biofuel industries, where xylanase with broad pH adaptability is a critical biocatalyst. This study also establishes a foundation for molecular engineering strategies, such as overexpression systems and site-directed mutagenesis, to further enhance the enzyme's catalytic efficiency and operational stability.

Supplementary Information The online version contains supplementary material available at https://doi.org/10.1007/s10123-026-00831-2.

Author contributions H.B isolated bacterial strain, performed the laboratory experiments and collected the data, A.S designed the study, isolated bacterial strains, performed the whole analysis and wrote the manuscript; M.S contributed to design the study and collect bacterial strains, R.M, M.F, and S.Z contributed to strains identification and reviewed the manuscript.

Funding Not applicable.

Data availability The *16S* rRNA genes sequence and the complete genome of strain S3 have been deposited in the NCBI database under accession numbers PQ774861, PQ774862, and PRJNA1199744 bioproject.

Declarations

Ethics approval and consent to participate Not applicable.

Consent for publication Not applicable.

Competing interests The authors declare no competing interests.

References

Ahmad Z, Butt M (2013) Partial purification and characterization of Xylanase produced from Aspergillus niger using wheat bran. Pakistan J Agric Sci 50:433–437

Almagro Armenteros JJ, Tsirigos KD, Sønderby CK, Petersen TN, Winther O, Brunak S, von Heijne G, Nielsen H (2019) SignalP 5.0 improves signal peptide predictions using deep neural networks. Nat Biotechnol 37:420–423

Alonge M, Lebeigle L, Kirsche M, Jenike K, Ou S, Aganezov S, Wang X, Lippman ZB, Schatz MC, Soyk S (2022) Automated assembly scaffolding using RagTag elevates a new tomato system for high-throughput genome editing. Genome Biol 23:258. https://doi.org/10.1186/s13059-022-02823-7

Amore A, Parameswaran B, Kumar R, Birolo L, Vinciguerra R, Marcolongo L, Ionata E, La Cara F, Pandey A, Faraco V (2015) Application of a new xylanase activity from Bacillus amyloliquefaciens XR44A in brewer's spent grain saccharification. J Chem Technol Biotechnol 90:573–581. https://doi.org/10.1002/jctb.4589

Bankevich A, Nurk S, Antipov D, Gurevich AA, Dvorkin M, Kulikov AS, Lesin VM, Nikolenko SI, Pham S, Prjibelski AD, Pyshkin AV, Sirotkin AV, Vyahhi N, Tesler G, Alekseyev MA, Pevzner PA (2012) SPAdes: a new genome assembly algorithm and its applications to single-cell sequencing. J Comput Biol J Comput Mol cell Biol 19:455–477. https://doi.org/10.1089/cmb.2012.0021

Beg Q, Kapoor M, Mahajan L, Hoondal G (2001) Microbial xylanases and their industrial applications: a review. Appl Microbiol Biotechnol 56:326–338. https://doi.org/10.1007/s002530100704

Bhalla A, Bischoff KM, Sani RK (2015) Highly Thermostable Xylanase Production from A Thermophilic Geobacillus sp. Strain WSUCF1 Utilizing Lignocellulosic Biomass. Front Bioeng Biotechnol 3:84. https://doi.org/10.3389/fbioe.2015.00084

Bhardwaj N, Kumar B, Verma P (2019) A detailed overview of xylanases: an emerging biomolecule for current and future prospective. Bioresour Bioprocess 6:40. https://doi.org/10.1186/s40643-019-0276-2

Bibi Z, Ansari A, Zohra RR, Aman A, Qader SA (2014) Production of xylan degrading endo-1 4-β-xylanase from thermophilic Geobacillus stearothermophilus KIBGE-IB29. J Radiation Res Appl Sci 7(4):478–485. https://doi.org/10.1016/j.jrras.2014.08.001

Biovia DS (2016) Dassault Systemes BIOVIA, Discovery Studio, 2019

Blin K, Shaw S, Steinke K, Villebro R, Ziemert N, Lee SY, Medema MH, Weber T (2019) antiSMASH 5.0: updates to the secondary metabolite genome mining pipeline. Nucleic Acids Res 47:W81–W87. https://doi.org/10.1093/nar/gkz310

Brown J, Pirrung M, McCue LA (2017) FQC Dashboard: integrates FastQC results into a web-based, interactive, and extensible FASTQ quality control tool. Bioinformatics 33:3137–3139. https://doi.org/10.1093/bioinformatics/btx373

Capella-Gutiérrez S, Silla-Martínez JM, Gabaldón T (2009) trimAl: a tool for automated alignment trimming in large-scale phylogenetic analyses. Bioinformatics 25:1972–1973. https://doi.org/10.1093/bioinformatics/btp348

Case RJ, Boucher Y, Dahllöf I, Holmström C, Doolittle WF, Kjelleberg S (2007) Use of 16S rRNA and rpoB genes as molecular markers for microbial ecology studies. Appl Environ Microbiol 73:278–288. https://doi.org/10.1128/AEM.01177-06

Chadha BS, Ajay BK, Mellon F, Bhat MK (2004) Two endoxylanases active and stable at alkaline pH from the newly isolated thermophilic fungus, Myceliophthora sp. IMI 387099. J Biotechnol 109:227–237. https://doi.org/10.1016/j.jbiotec.2003.12.010

Chakdar H, Kumar M, Pandiyan K, Singh A, Nanjappan K, Kashyap PL, Srivastava AK (2016) Bacterial xylanases: biology to biotechnology. 3 Biotech 6:150. https://doi.org/10.1007/s13205-016-0457-z

Chen KT, Lu CL (2018) CSAR-web: a web server of contig scaffolding using algebraic rearrangements. Nucleic Acids Res 46:W55–W59. https://doi.org/10.1093/nar/gky337

Chen Q, Li M, Wang X (2016) Enzymology properties of two different xylanases and their impacts on growth performance and intestinal microflora of weaned piglets. Anim Nutr 2:18–23. https://doi.org/10.1016/j.aninu.2016.02.003

Chen WP, Matsuo M, Yasui T (1986) Purification and some properties of β-1, 3-xylanase from Aspergillus terreus A-07. Agric Biol Chem 50:1183–1194

Christakopoulos P, Nerinckx W, Kekos D, Macris B, Claeyssens M (1996) Purification and characterization of two low molecular mass alkaline xylanases from Fusarium oxysporum F3. J Biotechnol 51:181–189. https://doi.org/10.1016/0168-1656(96)01619-7

Collins T, Gerday C, Feller G (2005) Xylanases, xylanase families and extremophilic xylanases. FEMS Microbiol Rev 29:3–23. https://doi.org/https://doi.org/ https://doi.org/10.1016/j.femsre.2004.06.005

Deng R-X, Wang W, Hu H-B, Zhang X (2025) Characterization and rational engineering of a novel thermostable xylanase from Streptomyces lomondensis S015 for enhanced properties. Int J Biol Macromol 149657

Dhaver P, Pletschke B, Sithole B, Govinden R (2022) Optimization, purification, and characterization of xylanase production by a newly isolated Trichoderma harzianum strain by a two-step statistical experimental design strategy. Sci Rep 12:17791. https://doi.org/10.1038/s41598-022-22723-x

Dheeran P, Nandhagopal N, Kumar S, Jaiswal YK, Adhikari DK (2012) A novel thermostable xylanase of Paenibacillus macerans IIPSP3 isolated from the termite gut. J Ind Microbiol Biotechnol 39:851–860. https://doi.org/10.1007/s10295-012-1093-1

Dodda SR, Hossain M, Kapoor BS, Dasgupta S, B VPR, Aikat K, Mukhopadhyay SS (2021) Computational approach for identification, characterization, three-dimensional structure modelling and machine learning-based thermostability prediction of xylanases from the genome of Aspergillus fumigatus. Comput Biol

Chem 91:107451. https://doi.org/10.1016/j.compbiolchem.2021.107451
Eberhardt J, Santos-Martins D, Tillack AF, Forli S (2021) AutoDock Vina 1.2.0: New Docking Methods, Expanded Force Field, and Python Bindings. J Chem Inf Model 61:3891–3898. https://doi.org/10.1021/acs.jcim.1c00203
Ebringerová A, Heinze T (2000) Xylan and xylan derivatives – biopolymers with valuable properties, 1. Naturally occurring xylans structures, isolation procedures and properties. Macromol Rapid Commun 21:542–556. https://doi.org/https:// https://doi.org/10.1002/1521-3927(20000601)21:9%3C542::AID-MARC542%3E3.0.CO;2-7
Edgar RC (2004) MUSCLE: multiple sequence alignment with high accuracy and high throughput. Nucleic Acids Res 32:1792–1797. https://doi.org/10.1093/nar/gkh340
Eisenberg D, Lüthy R, Bowie JU (1997) VERIFY3D: assessment of protein models with three-dimensional profiles. Methods Enzymol 277:396–404. https://doi.org/10.1016/s0076-6879(97)77022-8
Ellis JT, Magnuson TS (2012) Thermostable and Alkalistable Xylanases Produced by the Thermophilic Bacterium Anoxybacillus flavithermus TWXYL3. ISRN Microbiol 2012(517524). https://doi.org/10.5402/2012/517524
Gao Y, Zhu T, Zhang Z, Hu H, Wang Q, Liu H, Xiong L (2025) Characterization of a cold-active xylanase from Paenibacillus sp. XP01, and its application in hydrolyzing alkali-pretreated corncob residues. J Agric Food Chem 73:29751–29768
García-Huante Y, Cayetano-Cruz M, Santiago-Hernández A, Cano-Ramírez C, Marsch-Moreno R, Campos JE, Aguilar-Osorio G, Benitez-Cardoza CG, Trejo-Estrada S, Hidalgo-Lara ME (2017) The thermophilic biomass-degrading fungus Thielavia terrestris Co3Bag1 produces a hyperthermophilic and thermostable β-1,4-xylanase with exo- and endo-activity. Extremophiles 21:175–186. https://doi.org/10.1007/s00792-016-0893-z
Gasteiger E, Gattiker A, Hoogland C, Ivanyi I, Appel RD, Bairoch A (2003) ExPASy: The proteomics server for in-depth protein knowledge and analysis. Nucleic Acids Res 31:3784–3788. https://doi.org/10.1093/nar/gkg563
Gavande PV, Ji S, Cardoso V, Fontes MGA, Goyal C A (2024) Reassigning the role of a mesophilic xylan hydrolysing family GH43 β-xylosidase from Bacteroides ovatus, BoExXyl43A as exo-β-1,4-xylosidase. Curr Res Biotechnol 7:100191. https://doi.org/10.1016/j.crbiot.2024.100191
Hasan MA, Mazumder MHH, Chowdhury AS, Datta A, Khan MA (2015) Molecular-docking study of malaria drug target enzyme transketolase in Plasmodium falciparum 3D7 portends the novel approach to its treatment. Source Code Biol Med 10:7. https://doi.org/10.1186/s13029-015-0037-3
Heinze S, Mechelke M, Kornberger P, Liebl W, Schwarz WH, Zverlov VV (2017) Identification of endoxylanase XynE from Clostridium thermocellum as the first xylanase of glycoside hydrolase family GH141. Sci Rep 7:11178. https://doi.org/10.1038/s41598-017-11598-y
Hori C, Gaskell J, Igarashi K, Samejima M, Hibbett D, Henrissat B, Cullen D (2013) Genomewide analysis of polysaccharides degrading enzymes in 11 white- and brown-rot Polyporales provides insight into mechanisms of wood decay. Mycologia 105:1412–1427. https://doi.org/10.3852/13-072
Hung K-S, Liu S-M, Tzou W-S, Lin F-P, Pan C-L, Fang T-Y, Sun K-H, Tang S-J (2011) Characterization of a novel GH10 thermostable, halophilic xylanase from the marine bacterium Thermoanaerobacterium saccharolyticum NTOU1. Process Biochem 46:1257–1263. https://doi.org/10.1016/j.procbio.2011.02.009
Irfan M, Nadeem M, Syed Q, Baig S (2011) Effect of Medium Composition on Xylanase Production by Bacillus subtilis using Various Agricultural Wastes. Am-Eurasian J Agric Env Sci 12
Jalal A, Rashid N, Rasool N, Akhtar M (2009) Gene cloning and characterization of a xylanase from a newly isolated Bacillus subtilis strain R5. J Biosci Bioeng 107:360–365. https://doi.org/10.1016/j.jbiosc.2008.12.005
Jumper J, Evans R, Pritzel A, Green T, Figurnov M, Ronneberger O, Tunyasuvunakool K, Bates R, Žídek A, Potapenko A, Bridgland A, Meyer C, Kohl SAA, Ballard AJ, Cowie A, Romera-Paredes B, Nikolov S, Jain R, Adler J, Back T, Petersen S, Reiman D, Clancy E, Zielinski M, Steinegger M, Pacholska M, Berghammer T, Bodenstein S, Silver D, Vinyals O, Senior AW, Kavukcuoglu K, Kohli P, Hassabis D (2021) Highly accurate protein structure prediction with AlphaFold. Nature 596:583–589. https://doi.org/10.1038/s41586-021-03819-2
Kalogeris E, Christakopoulos P, Kekos D, Macris BJ (1998) Studies on the solid-state production of thermostable endoxylanases from Thermoascus aurantiacus: Characterization of two isozymes. J Biotechnol 60:155–163. https://doi.org/10.1016/S0168-1656(97)00186-7
Kamble RD, Jadhav AR (2012) Isolation, purification, and characterization of xylanase produced by a new species of bacillus in solid state fermentation. Int J Microbiol 2012:683193. https://doi.org/10.1155/2012/683193
Kasana RC, Salwan R, Dhar H, Dutt S, Gulati A (2008) A rapid and easy method for the detection of microbial cellulases on agar plates using gram's iodine. Curr Microbiol 57:503–507. https://doi.org/10.1007/s00284-008-9276-8
Kumar PS, Yaashikaa PR, Saravanan A (2018) Isolation, characterization and purification of xylanase producing bacteria from sea sediment. Biocatal Agric Biotechnol 13:299–303. https://doi.org/10.1016/j.bcab.2018.01.007
Lin H, Sun M-J, Li J-H, Xu Q-M, Yang B, Wang Q, Weijie X, Sun S-J, Hu K-H, Zhang L (2018) Purification and Characterization of Xylanase from Spent Mushroom Compost and its Application in Saccharification of Biomass Wastes. BioResources 13:220–230. https://doi.org/10.15376/biores.13.1.220-230
Liu N, Qin M, Gao Y, Li Z, Fu Y, Xu Q (2012) Pulp properties and fiber characteristics of xylanase-treated aspen APMP. BioResources 7
Li Y, Song W, Yin X, Rao S, Zhang Q, Zhou J, Li J, Du G, Liu S (2022) Enhanced catalytic performance of thermophilic GH11 xylanase by fusing carbohydrate-binding module 9−2 and linker for better synergistic degradation of wheat bran. Process Biochem 121:349–359. https://doi.org/10.1016/j.procbio.2022.07.021
Lo Leggio L, Parry NJ, Van Beeumen J, Claeyssens M, Bhat MK, Pickersgill RW (1997) Crystallization and preliminary X-ray analysis of the major endoglucanase from Thermoascus aurantiacus. Acta Crystallogr D Biol Crystallogr 53:599–604. https://doi.org/10.1107/S0907444997005404
Lombard V, Golaconda Ramulu H, Drula E, Coutinho PM, Henrissat B (2014) The carbohydrate-active enzymes database (CAZy) in 2013. Nucleic Acids Res 42:D490–D495. https://doi.org/10.1093/nar/gkt1178
Luong TTH, Poeaim S, Tangthirasunun N (2023) Isolation and Characterization of Xylanase from a Novel Strain, Penicillium menonorum SP10. Mycobiology 51:239–245. https://doi.org/10.1080/12298093.2023.2247221
Mai V, Wiegel J, Lorenz WW (2000) Cloning, sequencing, and characterization of the bifunctional xylosidase–arabinosidase from the anaerobic thermophile Thermoanaerobacter ethanolicus. Gene 247:137–143. https://doi.org/10.1016/S0378-1119(00)00106-2
Mamo G, Thunnissen M, Hatti-Kaul R, Mattiasson B (2009) An alkaline active xylanase: insights into mechanisms of high pH catalytic adaptation. Biochimie 91:1187–1196. https://doi.org/10.1016/j.biochi.2009.06.017
Meier-Kolthoff JP, Auch AF, Klenk H-P, Göker M (2013) Genome sequence-based species delimitation with confidence intervals

and improved distance functions. BMC Bioinformatics 14:60. https://doi.org/10.1186/1471-2105-14-60

Menon G, Mody K, Keshri J, Jha B (2010) Isolation, purification, and characterization of haloalkaline xylanase from a marine Bacillus pumilus strain, GESF-1. Biotechnol Bioprocess Eng 15:998–1005. https://doi.org/10.1007/s12257-010-0116-x

Mhiri S, Bouanane-Darenfed A, Jemli S, Neifar S, Ameri R, Mezghani M, Bouacem K, Jaouadi B, Bejar S (2020) A thermophilic and thermostable xylanase from Caldicoprobacter algeriensis: Recombinant expression, characterization and application in paper biobleaching. Int J Biol Macromol 164:808–817. https://doi.org/10.1016/j.ijbiomac.2020.07.162

Mittal A, Nagar S, Gupta VK (2013) Production and purification of high levels of cellulase-free bacterial xylanase by Bacillus sp. SV-34S using agro-residue. Ann Microbiol 63:1157–1167

Morais MAB, Coines J, Domingues MN, Pirolla RAS, Tonoli CCC, Santos CR, Correa JBL, Gozzo FC, Rovira C, Murakami MT (2021) Two distinct catalytic pathways for GH43 xylanolytic enzymes unveiled by X-ray and QM/MM simulations. Nat Commun 12:367. https://doi.org/10.1038/s41467-020-20620-3

Morana A, Paris O, Maurelli L, Rossi M, Cannio R (2007) Gene cloning and expression in Escherichia coli of a bi-functional beta-D-xylosidase/alpha-L-arabinosidase from Sulfolobus solfataricus involved in xylan degradation. Extremophiles 11:123–132. https://doi.org/10.1007/s00792-006-0020-7

Moreira LRS, Filho EXF (2016) Insights into the mechanism of enzymatic hydrolysis of xylan. Appl Microbiol Biotechnol 100:5205–5214. https://doi.org/10.1007/s00253-016-7555-z

Nagar S, Mittal A, Kumar D, Gupta VK (2012) Production of alkali tolerant cellulase free xylanase in high levels by Bacillus pumilus SV-205. Int J Biol Macromol 50:414–420. https://doi.org/10.1016/j.ijbiomac.2011.12.026

Nkohla A, Okaiyeto K, Olaniran A, Nwodo U, Mabinya L, Okoh A (2017) Optimization of growth parameters for cellulase and xylanase production by Bacillus species isolated from decaying biomass. J Biotech Res 8:33–47

Ogier J-C, Pagès S, Galan M, Barret M, Gaudriault S (2019) rpoB, a promising marker for analyzing the diversity of bacterial communities by amplicon sequencing. BMC Microbiol 19:171. https://doi.org/10.1186/s12866-019-1546-z

Pasalari A, Homaei A (2022) Isolation and Molecular Identification of Xylanase-Producing Bacteria from Ulva flexuosa of the Persian Gulf. Processes 10:1834. https://doi.org/10.3390/pr10091834

Paës G, Berrin J-G, Beaugrand J (2012) GH11 xylanases: Structure/function/properties relationships and applications. Biotechnol Adv 30:564–592. https://doi.org/10.1016/j.biotechadv.2011.10.003

Pereira de Almeida A, Vargas IP, Marciano CL, Zanoelo FF, Giannesi GC, Moraes Polizeli M, de LT JA, Furriel R dos, Ruller PM, Masui R DC (2022) Investigation of biochemical and biotechnological potential of a thermo-halo-alkali-tolerant endo-xylanase (GH11) from Humicola brevis var. thermoidea for lignocellulosic valorization of sugarcane biomass. Biocatal Agric Biotechnol 44:102424. https://doi.org/10.1016/j.bcab.2022.102424

Pettersen EF, Goddard TD, Huang CC, Couch GS, Greenblatt DM, Meng EC, Ferrin TE (2004) UCSF Chimera–a visualization system for exploratory research and analysis. J Comput Chem 25:1605–1612. https://doi.org/10.1002/jcc.20084

Pollet A, Delcour JA, Courtin CM (2010) Structural determinants of the substrate specificities of xylanases from different glycoside hydrolase families. Crit Rev Biotechnol 30:176–191. https://doi.org/10.3109/07388551003645599

Poosarla VG, Chandra TS (2014) Purification and characterization of novel halo-acid-alkali-thermo-stable xylanase from Gracilibacillus sp. TSCPVG Appl Biochem Biotechnol 173:1375–1390. https://doi.org/10.1007/s12010-014-0939-6

Prjibelski A, Antipov D, Meleshko D, Lapidus A, Korobeynikov A (2020) Using SPAdes De Novo Assembler. Curr Protoc Bioinforma 70:e102. https://doi.org/10.1002/cpbi.102

Putra A, Nathania A, Putri H, Febriyanti N, Komari N, Sanjaya R (2024) Structural and Molecular Dynamics Investigation of Bacterial and Fungal Xylanases. Indones J Chem Res 12:31–39. https://doi.org/10.30598/ijcr.2024.12-kom

Rahmani N, Kahar P, Lisdiyanti P, Lee J, Yopi, Prasetya B, Ogino C, Kondo A (2019) GH-10 and GH-11 Endo-1,4-β-xylanase enzymes from Kitasatospora sp. produce xylose and xylooligosaccharides from sugarcane bagasse with no xylose inhibition. Bioresour Technol 272:315–325. https://doi.org/10.1016/j.biortech.2018.10.007

Rausch T, Fritz MH-Y, Untergasser A, Benes V (2020) Tracy: basecalling, alignment, assembly and deconvolution of sanger chromatogram trace files. BMC Genomics 21:230. https://doi.org/10.1186/s12864-020-6635-8

Robledo A, Aguilar CN, Belmares-Cerda RE, Flores-Gallegos AC, Contreras-Esquivel JC, Montañez JC, Mussatto SI (2016) Production of thermostable xylanase by thermophilic fungal strains isolated from maize silage. CyTA - J Food 14:302–308. https://doi.org/10.1080/19476337.2015.1105298

Roy N, Habib MR (1970) Isolation and characterization of Xylanase producing strain of Bacillus cereus from soil. Iran J Microbiol 1

Saleem A, Waris S, Ahmed T, Tabassum R (2021) Biochemical characterization and molecular docking of cloned xylanase gene from Bacillus subtilis RTS expressed in E. coli. Int J Biol Macromol 168:310–321. https://doi.org/10.1016/j.ijbiomac.2020.12.001

Saleh MA, Mahmud S, Albogami S, El-Shehawi AM, Paul GK, Islam S, Dutta AK, Uddin MS, Zaman S (2022) Biochemical and Molecular Dynamics Study of a Novel GH 43 α-l-Arabinofuranosidase/β-Xylosidase From Caldicellulosiruptor saccharolyticus DSM8903. Front Bioeng Biotechnol 10:810542. https://doi.org/10.3389/fbioe.2022.810542

Sapkota A, Thapa A, Budhathoki A, Sainju M, Shrestha P, Aryal S (2020) Isolation, Characterization, and Screening of Antimicrobial-Producing Actinomycetes from Soil Samples. Int J Microbiol 2020:2716584. https://doi.org/10.1155/2020/2716584

Seemann T (2014) Prokka: rapid prokaryotic genome annotation. Bioinformatics 30:2068–2069. https://doi.org/10.1093/bioinformatics/btu153

Sen TZ, Jernigan RL, Garnier J, Kloczkowski A (2005) GOR V server for protein secondary structure prediction. Bioinformatics 21:2787–2788. https://doi.org/10.1093/bioinformatics/bti408

Shah S, Mallick BC, Devi B, Kumar M (2025) Exploring black soil microbiota for industrial enzymes: cellulase and xylanase characterization from Bacillus subtilis SSMK413. Microb Cell Fact. https://doi.org/10.1186/s12934-025-02898-4

Shanthi V, Roymon MG (2018) Isolation, Identification and Partial Optimization of Novel Xylanolytic Bacterial Isolates from Bhilai-Durg Region, Chhattisgarh, India. Iran J Biotechnol 16:e1333. https://doi.org/10.15171/ijb.1333

Sheik SS, Sundararajan P, Hussain ASZ, Sekar K (2002) Ramachandran plot on the web. Bioinformatics 18:1548–1549. https://doi.org/10.1093/bioinformatics/18.11.1548

Singh AK, Tripathi BM, Sahay H, Singh RN, Kaushik R, Saxena AK, Arora DK (2010) Biochemical and molecular characterization of thermo-alkali tolerant xylanase producing bacteria from thermal springs of Manikaran. Indian J Microbiol 50:2–9. https://doi.org/10.1007/s12088-010-0071-4

Song HY, Lim HK, Kim DR, Lee KI, Hwang IT (2014) A new bimodular endo-β-1,4-xylanase KRICT PX-3 from whole genome sequence of Paenibacillus terrae HPL-003. Enzyme Microb Technol 54:1–7. https://doi.org/10.1016/j.enzmictec.2013.09.002

Souza DT, Bispo ASR, Bon EPS, Coelho RRR, Nascimento RP (2012) Production of thermophilic endo-β-1,4-xylanases by Aspergillus

fumigatus FBSPE-05 using agro-industrial by-products. Appl Biochem Biotechnol 166:1575–1585. https://doi.org/10.1007/s12010-012-9563-5

Stamatakis A, Ludwig T, Meier H (2005) RAxML-III: a fast program for maximum likelihood-based inference of large phylogenetic trees. Bioinformatics 21:456–463. https://doi.org/10.1093/bioinformatics/bti191

Takita T, Nakatani K, Katano Y, Suzuki M, Kojima K, Saka N, Mikami B, Yatsunami R, Nakamura S, Yasukawa K (2019) Increase in the thermostability of GH11 xylanase XynJ from Bacillus sp. strain 41 M-1 using site saturation mutagenesis. Enzyme Microb Technol 130:109363. https://doi.org/10.1016/j.enzmictec.2019.109363

Tarafder S, Islam M, Shatabda S, Rahman A (2022) Figbird: a probabilistic method for filling gaps in genome assemblies. Bioinformatics 38:3717–3724. https://doi.org/10.1093/bioinformatics/btac404

Thomas L, Joseph A, Singhania RR, Patel AK, Pandey A (2017) In: Pandey A, Negi S, Soccol CRBT-CD in, B and B (eds) 6 - Industrial Enzymes: Xylanases. Elsevier, pp 127–148

Walia A, Mehta P, Chauhan A, Shirkot CK (2013) Optimization of cellulase-free xylanase production by alkalophilic Cellulosimicrobium sp. CKMX1 in solid-state fermentation of apple pomace using central composite design and response surface methodology. Ann Microbiol 63:187–198. https://doi.org/10.1007/s13213-012-0460-5

Wang D, Wu J, Du J, Xu X, Jiang S, Wang Y, Li T, Wang Y, Li T, Li C (2025) Thermostability Enhancement of the GH11 Xylanase XynZT-1 from Alteromonas macleodii HY35 Achieved via Modular Mosaic Engineering. J Agric Food Chem

William S, Feil H, Copeland A (2012) Bacterial genomic DNA isolation using CTAB. Sigma 50

Wu X, Zhang Q, Zhang L, Liu S, Chen G, Zhang H, Wang L (2020) Insights Into the Role of Exposed Surface Charged Residues in the Alkali-Tolerance of GH11 Xylanase. Front Microbiol 11:872. https://doi.org/10.3389/fmicb.2020.00872

Xin F, He J (2013) Characterization of a thermostable xylanase from a newly isolated Kluyvera species and its application for biobutanol production. Bioresour Technol 135:309–315. https://doi.org/10.1016/j.biortech.2012.10.002

Xiong K, Yan Zxiang, Liu J, yun, Pei P gang, Deng L, Gao L, Sun Bguo (2020) Inter domain interactions influence the substrate affinity and hydrolysis product specificity of xylanase from Streptomyces chartreusis L1105. Ann Microbiol 70:19. https://doi.org/10.1186/s13213-020-01560-1

Yagi H, Takehara R, Tamaki A, Teramoto K, Tsutsui S, Kaneko S (2019) Functional Characterization of the GH10 and GH11 Xylanases from Streptomyces olivaceoviridis E-86 Provide Insights into the Advantage of GH11 Xylanase in Catalyzing Biomass Degradation. J Appl Glycosci 66:29–35. https://doi.org/10.5458/jag.jag.JAG-2018_0008

Yang H, Yi N, Zhao S, Qaseem MF, Zheng B, Li H, Feng J-X, Wu A (2020a) Characterization of hemicelluloses in sugarcane (Saccharum spp. hybrids) culm during xylogenesis. Int J Biol Macromol 165:1119–1128. https://doi.org/10.1016/j.ijbiomac.2020.09.242

Yang J, Han Z (2018) Understanding the Positional Binding and Substrate Interaction of a Highly Thermostable GH10 Xylanase from Thermotoga maritima by Molecular Docking. Biomolecules 8

Yang J, Ma T, Shang-Guan F, Han Z (2020b) Improving the catalytic activity of thermostable xylanase from Thermotoga maritima via mutagenesis of non-catalytic residues at glycone subsites. Enzyme Microb Technol 139:109579. https://doi.org/10.1016/j.enzmictec.2020.109579

Zarafeta D, Galanopoulou AP, Leni ME, Kaili SI, Chegkazi MS, Chrysina ED, Kolisis FN, Hatzinikolaou DG, Skretas G (2020) XynDZ5: A New Thermostable GH10 Xylanase. Front Microbiol 11:545. https://doi.org/10.3389/fmicb.2020.00545

Zhang S, Zhao S, Shang W, Yan Z, Wu X, Li Y, Chen G, Liu X, Wang L (2021) Synergistic mechanism of GH11 xylanases with different action modes from Aspergillus niger An76. Biotechnol Biofuels 14:118. https://doi.org/10.1186/s13068-021-01967-1

Zhao L, Meng K, Shi P, Bai Y, Luo H, Huang H, Wang Y, Yang P, Yao B (2013) A novel thermophilic xylanase from Achaetomium sp. Xz-8 with high catalytic efficiency and application potentials in the brewing and other industries. Process Biochem 48:1879–1885. https://doi.org/10.1016/j.procbio.2013.08.020

Zheng F, Basit A, Zhuang H, Chen J, Zhang J, Chen W (2022) Biochemical characterization of a novel acidophilic β-xylanase from Trichoderma asperellum ND-1 and its synergistic hydrolysis of beechwood xylan. Front Microbiol 13:998160. https://doi.org/10.3389/fmicb.2022.998160